

Superfunctional high-entropy alloys and ceramics by severe plastic deformation

Parisa Edalati^{1,2,*}, Masayoshi Fuji^{1,2,*} and Kaveh Edalati^{3,4,*}

¹ Department of Life Science and Applied Chemistry, Nagoya Institute of Technology, Tajimi 507-0071, Japan

² Advanced Ceramics Research Center, Nagoya Institute of Technology, Tajimi 507-0071, Japan

³ WPI International Institute for Carbon-Neutral Energy Research (WPI-I2CNER), Kyushu University, Fukuoka 819-0395, Japan

⁴ Mitsui Chemicals, Inc.—Carbon Neutral Research Center (MCI-CNRC), Kyushu University, Fukuoka 819-0395, Japan

High-entropy alloys and ceramics containing at least five principal elements have recently received high attention for various mechanical and functional applications. The application of severe plastic deformation (SPD), particularly the high-pressure torsion (HPT) method, combined with the CALPHAD and first-principles calculations resulted in the development of numerous superfunctional high-entropy materials with superior properties compared to the normal functions of engineering materials. This article reviews the recent advances in the application of SPD to developing superfunctional high-entropy materials. These superfunctional properties include (i) ultrahigh hardness levels comparable to the hardness of ceramics in high-entropy alloys, (ii) high yield strength and good hydrogen embrittlement resistance in high-entropy alloys; (iii) high strength, low elastic modulus, and high biocompatibility in high-entropy alloys, (iv) fast and reversible hydrogen storage in high-entropy hydrides, (v) photovoltaic performance and photocurrent generation on high-entropy semiconductors, (vi) photocatalytic oxygen and hydrogen production from water splitting on high-entropy oxides and oxynitrides, and (vii) CO₂ photoreduction on high-entropy ceramics. These findings introduce SPD as not only a processing tool to improve the properties of existing high-entropy materials but also as a synthesis tool to produce novel high-entropy materials with superior properties compared with conventional engineering materials.

Keywords: multi-principal element alloys (MPEAs); high-entropy alloys (HEAs); high-entropy ceramics (HECs); high-entropy oxides (HEOs); ultrafine-grained (UFG) microstructure; high-pressure torsion (HPT).

* Corresponding authors: P. Edalati (E-mail: parisaedalati@gmail.com; Tel: +81-57-224-8110)
M. Fuji (E-mail: fuji@nitech.ac.jp; Tel: +81-57-224-8110)
K. Edalati (E-mail: kaveh.edalati@kyudai.jp; Tel: +81-92-802-6744)

1. Introduction

There have been significant activities within the past three decades to produce bulk ultrafine-grained (UFG) materials using severe plastic deformation (SPD) methods such as high-pressure torsion (HPT), equal-channel angular pressing (ECAP), accumulative roll-bonding (ARB), twist extrusion (TE), and multidirectional forging (MDF) [1-4]. The formation of UFG structures with a large density of lattice defects leads to exceptional mechanical and functional properties of these severely deformed materials [5-8]. Since the properties of these materials are superior to conventional engineering materials, a recent publication used the term superfunctional materials for them [9]. Although SPD was well-known in western countries several decades ago [10-12], the method owes its popularity to a few interesting works done by Russian scientists in the 1980s [13,14].

A special issue edited by Edalati and Horita in 2019 reviewed the historical developments and recent advances in the SPD field by inviting the most active scientists in the field [15,16]. These review papers covered a wide range of progress from the mechanism and theoretical aspects of SPD [17-20] to the processing aspects including traditional SPD methods [20-23] continuous methods [24], upscaled methods [25,26], *in situ* methods [19,27], and surface treatment methods [28,29]. Although SPD was defined as a metal processing method at the beginning of this century, its application has been currently extended to non-metallic materials by several research groups [19,27,30-33]. These review papers clearly confirm that the SPD methods are widely used by researchers from many countries to control microstructural features/defects [34-38] and solid-state phase transformations [39-42] to achieve a wide range of mechanical [43-48] and functional properties [32,49-56].

In recent years, many publications reported the application of the SPD process to high-entropy or multi-principal element materials, although these publications were not reviewed in the above-mentioned special issue. High-entropy materials, including high-entropy alloys [57-59] and high-entropy ceramics [60-62], which were first introduced in 2004 [63,64], are compounds containing at least five principal elements (5-35 at%) with a configurational entropy higher than $1.5R$ (R : gas constant). High-entropy materials show promising properties mainly because of the cocktail effect, lattice distortion, sluggish diffusion, and high configurational entropy [57-62]. The SPD methods were successfully used not only as a processing tool to enhance the properties of high-entropy alloys but also as a synthesis tool to develop new high-entropy alloys and ceramics [65].

A summary of publications on the application of SPD to medium-entropy and high-entropy materials is given in Table A1 of the Appendix [66-169]. While most studies focused on microstructural features and mechanical properties, there are limited studies on functional properties. This article reviews the recent advances in the application of SPD to achieve superfunctional high-entropy materials.

2. Ultrahigh hardness

The most investigated properties of high-entropy alloys are mechanical properties [5,6], and it is believed these materials can have a higher hardness than conventional engineering alloys [170,171]. The high hardness is usually attributed to lattice strain and significant solution hardening in these alloys [170-173]. The introduction of these alloys resulted in some attempts to design metallic alloys with hardness levels comparable to brittle ceramics. A few studies designed new high-entropy alloys and processed them by HPT to achieve some of the highest hardness levels ever reported in metallic alloys. Carbon-doped AlTiFeCoNi is an alloy designed by using

the thermodynamic calculations using CALPHAD (calculation of phase diagram) to have dual phases with some small amounts of carbide precipitate, as shown in Fig. 1a [136]. The alloy shows an ultrahigh hardness of 950 Hv after SPD processing, as shown in Fig. 1b. Such a high hardness was not only due to the high solution hardening effect but also due to some other hardening mechanisms such as the formation of nanograins with sizes smaller than 100 nm, interphase hardening shown in Fig. 1c, dislocation accumulation shown in Fig. 1d, and precipitation hardening [136]. The formation of nanograins with sizes smaller than 100 nm, which cannot be easily achieved in severely deformed metals and conventional alloys, should be due to the significant interaction of solute atoms with dislocations and grain boundaries in high-entropy alloys.

In another study, one of the highest hardness levels reported for metallic alloys (1030 Hv) was achieved in a newly designed dual-phase (cubic + hexagonal) AlCrFeCoNiNb alloy, as shown in Fig. 1e [17]. The introduction of 10 nm nanograin sizes (Fig. 1f), dislocations (Fig. 1g), interfaces, and spinodal decomposition were responsible for such a high hardness [137]. In summary, the SPD process can be used to produce high-entropy alloys with ultrahigh hardness levels comparable to ceramics, while the plasticity of alloys is naturally higher than ceramics. Here, it should be noted that processing of such ultrahard alloys is currently possible only by HPT. Since a disc or ring is torsionally strained under very high pressures in HPT [174,175], the method is applicable to hard and less ductile materials including metals (Hf [176], Mo [177], and W [178]), glasses [179,180], silicon [181,182] and even diamond [183,184]. Another issue that needs to be considered is that the authors' attempt to apply SPD to existing single-phase [166] and dual-phase [163] high-entropy alloys led to hardness values that were not comparable to those of carbon-doped AlTiFeCoNi and AlCrFeCoNiNb, and thus, the design of alloys to have the simultaneous contribution of different hardening mechanisms is essential for achieving ultrahigh hardness after SPD [136,137].

These studies clearly show that the combination of various strengthening mechanisms in high-entropy alloys by SPD processing is a new strategy to realize metallic materials with high hardness levels comparable to the hardness of ceramics. Although metallic materials are expected to exhibit higher plasticity compared to ceramics, it is essential to conduct future research on the enhancement of the ductility of these ultrahard high-entropy alloys to have a good combination of ultrahigh hardness and high ductility.

3. Hydrogen embrittlement resistance

With the quick development of hydrogen as a clean fuel, demand for materials that show high strength in the presence of hydrogen has increased [185]. The main drawback in this regard is that high-strength alloys, such as steels with martensitic or body-centered cubic (BCC) structures, show poor plasticity in the presence of hydrogen due to different hydrogen embrittlement mechanisms such as hydrogen-enhanced localized plasticity [186] or hydrogen-enhanced decohesion [187]. Although all materials basically suffer from hydrogen embrittlement, the alloys with face-centered cubic (FCC) crystal structures like austenitic steels have more compatibility with hydrogen [188,189]. Recently, high-entropy alloys with the FCC crystal structure, particularly CrMnFeCoNi Cantor alloy, were introduced as new hydrogen-compatible materials [190,191]; however, these alloys have low yield strength.

A recent study employed the HPT method to enhance the yield strength of Cantor alloy and examine its hydrogen embrittlement resistance after applying various levels of strains (i.e. after various HPT turns), as shown in Fig. 2a [167]. Although coarse-grained material exhibits a

large elongation of about 80% in the presence of hydrogen, its yield stress is 220 MPa which is not a high strength for many engineering applications. When low levels of strain are applied to the material such as 1/16 rotations of HPT, large fractions of twins are formed (Fig. 2b), leading to more than 1 GPa yield stress in the presence of hydrogen with an appreciable elongation of about 9%. With a further increase in the applied strain such as 1/8-1/4 rotations of HPT, dislocation-based defects, particularly low-mobility Lomer-Cottrell locks (Fig. 2c) and D-Frank partial dislocations (Fig. 2d), are generated which can further enhance the yield strength, while retaining acceptable plasticity. With a significant increase in strain such as 1-10 HPT rotations, nanograins are formed leading to up to 1.9 GPa strength but with very poor resistance to hydrogen embrittlement due to the possible occurrence of hydrogen-enhanced decohesion at grain boundaries.

Another study applied SPD to the surface through surface mechanical attrition treatment (SMAT) and reported a combination of high yield stress (0.5-0.7 GPa) and high plasticity (15-33%) in the presence of hydrogen (Fig. 2e) [165]. Such impressive results were attributed to the formation of gradient microstructure with a large fraction of twins (Fig. 2f). These studies suggested that twins and low-mobility Lomer-Cottrell locks and D-Frank partial dislocations are appropriate defects in the Cantor alloy to obtain large yield strength and good plasticity due to the suppression of hydrogen-enhanced localized plasticity [165,167]. However, the formation of nanograins leads to poor hydrogen embrittlement resistance of the Cantor alloy due to fast grain-boundary hydrogen diffusion and domination of hydrogen-enhanced decohesion [165,167]. Although poor ductility is a well-known feature of many metallic nanomaterials which needs to be improved using special strategies [192-196], this effect seems to be more severe in the presence of hydrogen in high-entropy alloys leading to failure even in the elastic region [165,167].

These studies suggest that high-entropy alloys have a high potential to achieve a combination of high strength and high hydrogen embrittlement resistance by controlling the lattice defects through SPD processing. However, the strength level and resistance to embrittlement can be still improved by controlling the chemical composition of these alloys to suppress the diffusion of hydrogen through the surface to bulk as well as through the lattice. Moreover, a combination of the SPD process and heat treatment can be used for further engineering of lattice defects and controlling their interaction with hydrogen.

4. Biocompatibility

Severely deformed materials, particularly titanium and its alloys, can exhibit a good combination of high strength and good biocompatibility [197-199], and this has led to the commercialization of these materials for biomedical applications [200]. However, for materials used as implants for orthopedics, besides high strength and biocompatibility, the elastic modulus should be low and ideally comparable to the elastic modulus of human bone (10-30 GPa) [201]. Recently, high-entropy alloys were introduced as a new family of biocompatible materials with reasonable elastic modulus [202-205], but the strength of these materials needs to be enhanced by appropriate hardening mechanisms [206-210].

In a study, a lattice-softened Ti-containing high-entropy alloy, TiAlFeNiCo, was designed with the aid of thermodynamic calculations and further processed by SPD through the HPT method to enhance its strength [123]. The material had a coarse-grained structure with the BCC + L2₁ crystal structure after arc melting, but it showed phase transformation to the BCC phase after HPT processing together with the formation of UFG structure. These structural and microstructural modifications by HPT processing resulted in the enhancement of hardness and the reduction of

elastic modulus to about 120 GPa, as shown in the plots of nanoindentation load against displacement in Fig. 3a. A comparison between the strength (examined by Vickers method) and cell proliferation-viability-cytotoxicity activity (examined by MTT assay) of this high-entropy alloy with those achieved for pure titanium and the Ti-6Al-7Nb (wt%) alloy is shown in Fig. 3b. The TiAlFeCoNi alloy shows 170-580% larger microhardness and 260-1020% higher cellular metabolic activity than pure titanium and the Ti-6Al-7Nb alloy, while its elastic modulus is similar to these two biomaterials [123].

Biocompatible high-entropy alloys can be also synthesized from the powders of pure metals by using the concept of ultra-SPD [134]. In ultra-SPD, the shear strain is significantly enhanced (usually over 1,000) so that the thickness of sheared phases becomes geometrically comparable to atomic distances [211]. Ultra-SPD is quite effective to synthesize a wide range of alloys even from immiscible systems [212-214] not only because of the mechanical strain effect but also due to ultrafast dynamic diffusion [215-217]. Among various SPD methods, HPT is currently the best method to impart ultra-SPD because the method can induce very large strains (only by continuous rotation of HPT anvils) without any contamination or significant temperature rise [218,219]. Therefore, the HPT method can be used to simultaneously conduct mechanical alloying, consolidate the powders at low temperatures and refine the grain size to the UFG region [212-214]. A recent study directly synthesized several biomaterials from the powders of pure metals by the concept of ultra-SPD: a binary TiNb alloy, a ternary TiNbZr alloy, a medium-entropy alloy TiNbZrTa, and a high-entropy alloy TiNbZrTaHf [134]. All synthesized biomaterials had single BCC phases with grain sizes at the nanometer level. As shown in Fig. 3c, the hardness increases with increasing the number of principal elements, while the high-entropy alloy with five principal elements exhibits the highest hardness. As shown in Fig. 3d, these medium-entropy and high-entropy alloys have elastic modulus values close to 80 GPa, which is comparable to or even better than many commercial biomaterials, while their hardness levels are almost the highest for the biocompatible alloys (> 500 Hv). In conclusion, a combination of the concepts of SPD and high-entropy materials appears as a promising approach to developing biomaterials with high strength, low elastic modulus, and good biocompatibility [123,134]. Corrosion resistance, deformation ductility, fatigue properties, and tribological properties are other critical parameters that need to be investigated for the practical application of SPD-processed high-entropy materials for biomedical applications [220], although a study reported good corrosion resistance of these alloys after SPD processing [150].

A good combination of high strength and high biocompatibility of severely deformed high-entropy alloys compared to conventional biomaterials introduces them as a new family of biomaterials. However, the future direction should be the design of alloys with appropriate density and a lower elastic modulus. Moreover, although aluminum is still used in biomedical alloys such as Ti-6V-4Al and Ti-6Al-7Nb (wt%), this element should be excluded from the composition of conventional and high-entropy alloys in the future because of biomedical toxicity issues.

5. Hydrogen storage

Hydrogen is considered a clean fuel for the future, but since hydrogen is a light gas, its safe and high-density storage is a big academic and industrial challenge [221]. Metal hydrides provide a promising technology for compact and low-pressure storage of hydrogen [222,223]; however, many hydrides suffer either from kinetic issues (i.e., activation and hydrogenation/dehydrogenation rate) or thermodynamic issues (i.e., the high stability of hydride at room temperature) [224,225]. The SPD methods, particularly ECAP [226-228] and HPT [229-

[231], were successfully used to solve the kinetic issues of metal hydrides by mechanochemistry [232]. Moreover, there is a successful attempt to solve the thermodynamic aspects of metal hydrides by using the concepts of binding-energy engineering and ultra-SPD which resulted in the discovery of the first Mg-based alloy for reversible hydrogen storage at room temperature [233]. Similar concepts were employed to discover new high-entropy materials with the capability to store hydrogen at room temperature. The first attempt was synthesizing MgTiVCrFe by SPD which resulted in the BCC + amorphous structure with poor hydrogen storage at room temperature [117]. The second attempt was TiZrCrMnFeNi with the C14 Laves phase structure, which was originally synthesized by SPD but later could be synthesized by conventional arc melting [113]. These studies were later employed to design other high-entropy alloys for low/room-temperature hydrogen storage such as TiZrNbFeNi [234], TiZrNbCrFe [235] and $\text{Ti}_x\text{Zr}_{2-x}\text{CrMnFeNi}$ ($x = 0.4-1.6$) [236].

The high-entropy hydrogen storage materials were designed based on three criteria [113]. (i) The AB_2 system is the most appropriate to have low hydrogen binding energy, where A denotes the hydride-forming metals like magnesium, titanium, zirconium, vanadium, and niobium, and B denotes metals with low affinity with the hydrogen atoms like chromium, manganese, iron, cobalt, and nickel. (ii) The average valence electron concentration should be close to 6.4. (iii) The C14 Laves phase has the highest possibility for room-temperature hydrogen storage. The use of these criteria is expected to lead to a hydrogen binding energy slightly lower than 0.1 eV which is a target for reversible room-temperature hydrogen storage, as shown in Fig. 4a [236]. For the AB_2 -type TiZrCrMnFeNi with a valence electron concentration of 6.4, the CALPHAD calculations confirmed the theoretical stability of the C14 Laves phase structure [113] and first-principles calculations confirmed an appropriate hydrogen binding energy of close to -0.1 eV, as shown in Figs. 4b and 4c [236]. The synthesized TiZrCrMnFeNi alloy with an equiatomic fraction of elements exhibited a C14 Laves phase structure with reversible room-temperature hydrogen storage of 1.7 wt% (30% higher capacity compared to commercial LaNi_5), as shown in Fig. 3d [113]. The hydrogenation kinetics of the alloy was also good, it absorbed hydrogen without any need for an activation process, and its hydrogenation rate was very fast, as shown in Fig. 3e [113]. Moreover, the TiZrCrMnFeNi alloy could be handled under an air atmosphere, while hydrogen storage materials should be usually handled under a controlled atmosphere (e.g., in a glove box). Moreover, the examination of cyclic stability, conducted for a non-equiatomic alloy $\text{Ti}_{0.4}\text{Zr}_{1.6}\text{CrMnFeNi}$, confirmed excellent cycling stability for at least 1,000 cycles without any loss in the storage capacity, as shown in Fig. 4f [236]. The room-temperature hydrogen storage capability of $\text{Ti}_x\text{Zr}_{2-x}\text{CrMnFeNi}$ ($x = 0.4-1.6$) alloys resulted in the first experimental application of high-entropy alloys as the anode material of nickel-metal hydride (Ni-MH) batteries, although the discharge capacity of these alloys was not as high as the commercial Ni-MH batteries [237].

In conclusion, the high-entropy alloys, designed by binding-energy engineering and primarily synthesized by SPD, have introduced new candidates for fast and reversible hydrogen storage at room temperature with capacities larger than commercial hydrogen storage materials such as LaNi_5 . These materials are currently designed by using transition metals to have a C14 Laves crystal structure with a hydrogen-to-metal atomic ratio of 1, but future studies are expected to focus on the design of high-entropy alloys with higher hydrogen-to-metal atomic ratios such as the BCC alloys and on the use of lighter elements. The employment of theoretical concepts is essential for the future design of such high-entropy hydrogen storage materials.

6. Photovoltaics

Photovoltaics, which is used in solar cells, is defined as the conversion of light to electric current using semiconductors [238]. Currently, silicon and GaAs show the highest efficiency to generate photocurrent [239,240], but there are significant efforts all over the world to discover new semiconductors for such applications. The high-entropy ceramics, including TiZrHfNbTaO_{11} [126,155] and $\text{TiZrHfNbTaO}_6\text{N}_3$ [127,154] semiconductors, are one of the newest families of photovoltaic materials synthesized by SPD. These materials were synthesized from elemental metallic powders by HPT and subjected to oxidation and nitriding to produce high-entropy oxides and oxynitrides, respectively. These high-entropy materials were used in the form of thin films by deposition on fluorine-doped tin oxide glass and used photocurrent generation. Fig. 5a shows the appearance of TiZrHfNbTaO_{11} powder [126], Fig. 5b shows its microstructures [126], and Fig. 5c shows its photocurrent generation [155]. It is evident that the oxide can generate electric current under light, although its efficiency is not still comparable to conventional photovoltaic materials. One reason for the low efficiency of this semiconductor is the technical difficulty in fabricating a dense thin film, an issue that needs to be addressed in future studies. Despite this technical difficulty, SPD contributed to the field of photovoltaics by introducing not only high-entropy semiconductors [126,127,154,155] but also some other semiconductors such as high-pressure TiO_2 -II columbite phase [241] and black Bi_2O_3 [242].

Although the efficiency of SPD-synthesized high-entropy ceramic for photocurrent generation is still lower than commercial silicon and GaAs materials, research on this issue is still in its early stages. Future studies should focus not only on the design and synthesis of effective semiconductors for photovoltaics but also on using effective technologies to make dense thin films from these high-entropy semiconductors.

7. Photocatalytic water splitting

Photocatalysis is a clean technology to produce hydrogen from water splitting under solar energy in the presence of a light-absorbing catalyst such as TiO_2 [243,244]. Despite high scientific interest in photocatalytic hydrogen production, the efficiency of the method is still low for practical applications, and thus, there is a high demand to discover new photocatalysts with high activity [243,244]. A good photocatalyst should have some features such as large light absorbance, appropriate band structure compared to potentials for hydrogen and oxygen production, low bandgap, slow electron-hole recombination rate, a large fraction of active sites on the surface, and high chemical stability [245]. High-entropy photocatalysts were recently introduced as a new family of materials for photocatalytic water splitting [126,127,160]. High-entropy ceramics - which were also used as catalysts for electrocatalytic O_2 generation [246-248], chemical oxidation of CO [249-251], operation of lithium-sulfur batteries [252], electrocatalytic CO_2 conversion [253], operation of electrochemical capacitors [254], and chemical combustion reactions [255] - have some features that make them attractive as catalysts [256]. (i) They have low free Gibbs energy which gives them high chemical stability. (ii) They have a large fraction of inherent surface defects as active sites for photocatalysis. (iii) The band structure and bandgap of these materials can be adjusted easier than conventional photocatalysts by changing the type or fraction of principal elements.

TiZrHfNbTaO_{11} is the first high-entropy oxide photocatalyst which was synthesized by HPT processing followed by oxidation for photocatalytic hydrogen production [126]. The second material was high-entropy oxynitride photocatalyst $\text{TiZrHfNbTaO}_6\text{N}_3$ synthesized by a three-step process including HPT processing, oxidation, and high-temperature nitriding [127]. As shown in Fig. 6a, the materials show higher light absorbance compared to all binary oxides and high-entropy

oxides in the Ti-Zr-Hf-Nb-Ta system. The material shows high stability for photocatalytic hydrogen production, and it remains active for at least six months (Fig. 6b), while low stability is a general drawback of low-bandgap nitrides and oxynitrides [245]. In the most recent attempt, TiZrNbTaWO₁₂ with ten different kinds of heterojunctions (i.e., interphase boundaries which can ease electron-hole separation and migration) was produced by HPT processing followed by oxidation [160]. TiZrNbTaWO₁₂ could produce oxygen from water under visible light (Fig. 6c), while the activity of most photocatalysts is limited to the ultraviolet (UV) range of sunlight [243,244].

In conclusion, high-entropy photocatalysts, which were first synthesized by SPD, show high potential for water splitting and it is expected that a wider range of compositions and different synthesis methods will be employed in the future to utilize these materials. The key point in this respect is the design of active photocatalysts through the use of theoretical concepts. Moreover, some technologies should be employed to increase the surface area of these high-entropy photocatalysts by producing nanopowders.

8. CO₂ photoreduction

CO₂ emission from human activity has made the serious problem of global warming, an issue that is expected to influence the lives of many people in the 21st century [257]. In addition to the utilization of zero-CO₂ emission fuels such as hydrogen, the capture of CO₂ and its conversion to reactive gases such as CO or value-added hydrocarbons and fuels is another solution to deal with the CO₂ emission issues [258]. Photoreduction of CO₂ under sunlight and in the presence of a semiconductor catalyst is the cleanest technology for such conversions, but the field is rather new and needs significant improvement particularly by discovering new catalysts [259]. The SPD method was effectively used to improve CO₂ photoreduction by inducing high-pressure phases and oxygen vacancies in typical photocatalysts such as TiO₂ [260] and BiVO₄ [261]. The introduction of high-entropy oxides and oxynitrides, synthesized by SPD, is another successful attempt in this regard [154,155].

The band structure and the position of the valence band top and the conduction band bottom for TiZrHfNbTaO₁₁ and TiZrHfNbTaO₆N₃, which were originally designed and synthesized for photocatalytic water splitting [126,127], satisfy the energy requirements for CO₂ photoreduction, as shown in Fig. 7a [154]. While the high-entropy oxide has a bandgap of 3 eV which is similar to TiO₂, the high-entropy oxynitride shows a low bandgap of 1.6 eV. In addition to low bandgap and appropriate band structure, physical adsorption and chemisorption of CO₂ on high-entropy catalysts, particularly on TiZrHfNbTaO₆N₃, is higher than TiO₂, as shown in Fig. 7b using diffuse reflectance infrared Fourier transform spectroscopy [154]. Moreover, photoluminescence measurements suggest lower electron-hole recombination in this oxynitride compared to relevant high-entropy oxide and TiO₂ [154]. TiZrHfNbTaO₁₁ shows high activity for CO₂ photoreduction compared to P25 TiO₂ which is a benchmark catalyst, while TiZrHfNbTaO₆N₃ exhibits even higher CO₂ photoreduction activity, as shown in Fig. 7c [154].

These preliminary studies confirm the contribution of SPD in introducing some of the most active catalysts for CO₂ photoreduction by using the concept of high-entropy ceramics. Despite significant success in the experimental development of such ceramics, theoretical calculations are needed to clarify the mechanisms underlying their high activity. CALPHAD, density functional theory calculations, molecular dynamics simulations, and multiscale modeling are some approaches that can shed light on understanding the mechanism of activity of these new catalysts and their mechanochemistry by SPD processing [262-264].

9. Concluding remarks and future outlook

Superfunctional high-entropy alloys and ceramics, with properties superior to the normal functions of engineering materials, can be developed by processing or synthesizing through severe plastic deformation (SPD). The SPD has led to various superfunctional properties including (i) ultrahigh hardness, (ii) high strength with good hydrogen embrittlement resistance, (iii) high strength, and biocompatibility with low elastic modulus, (iv) fast and reversible room-temperature hydrogen storage, (v) photocurrent generation, (vi) photocatalytic water splitting, and (vii) CO₂ photoreduction. These findings not only suggest new applications for SPD but also introduce severely deformed high-entropy alloys and ceramics as a new family of superfunctional materials with high potential for various applications. The application of severely deformed high-entropy materials is expected to be expanded by considering the current demands to discover advanced energy materials with higher efficiency.

Acknowledgments

The author P.E. thanks the Hosokawa Powder Technology Foundation of Japan for a grant. The author K.E. was supported by the MEXT, Japan through Grants-in-Aid for Scientific Research on Innovative Areas (JP19H05176 & JP21H00150), and in part by the MEXT, Japan through Grant-in-Aid for Challenging Research Exploratory (JP22K18737).

Appendix

Table A1 summarizes the publications on the application of SPD as a processing or synthesis tool to medium-entropy materials (containing four principal elements) and high-entropy materials (containing at least five principal elements) [66-169].

Table A1. Summary of publications about severe plastic deformation of medium- and high-entropy alloys and ceramics in chronological order.

Composition	Crystal Structure	SPD Method	SPD Role	Properties or Features	References
AlCoCrCuFeNi	BCC + FCC	MDF	Processing	Superplasticity	Kuznetsov <i>et al.</i> (2013) [66]
AlFeMgTiZn	Multiphases	ECAP	Processing	Mechanical properties	Hammond <i>et al.</i> (2014) [67]
CoCrFeHMnNi	FCC	HPT	Processing	Mechanical properties and thermal stability	Schuh <i>et al.</i> (2015) [68]
Al _{0.3} CoCrFeNi	FCC	HPT	Processing	Hardening by straining and annealing	Tang <i>et al.</i> (2015) [69]
CoCrFeNiMn	FCC	HPT	Processing	Nanomechanical behavior	Lee <i>et al.</i> (2015) [70]
Al _{0.3} CoCrFeNi	FCC	HPT	Processing	Microstructural features	Tang <i>et al.</i> (2015) [71]
Al _{0.1} CoCrFeNi	FCC	HPT	Processing	Microstructural features	Yu <i>et al.</i> (2016) [72]
Al _{0.3} CoCrFeNi	FCC	HPT	Processing	Annealing-induced phase transformation	Tang <i>et al.</i> (2016) [73]
CoCrFeMnNi	FCC	HPT	Processing	Nanoindentation creep behavior	Lee <i>et al.</i> (2016) [74]
CoCrFeNiMn	FCC	HPT	Processing	Annealing effect on mechanical properties	Shahmir <i>et al.</i> (2016) [75]
Al _{0.3} Cu _{0.5} CoCrFeNi	FCC	HPT	Processing	Strain-induced homogenization	Yuan <i>et al.</i> (2016) [76]
Ti ₃₅ Zr _{27.5} Hf _{27.5} Nb ₅ Ta ₅	HCP	HPT	Processing	Microstructure and hardness	Heczal <i>et al.</i> (2017) [77]
CrMnFeCoNi	FCC	HPT	Processing	Phase stability examination by nanoindentation	Maier-Kiener <i>et al.</i> (2017) [78]

CoCrFeNiMn	FCC	HPT	Processing	Superplasticity	Shahmir et al. (2017) [79]
AlTiVNb	BCC	HPT	Processing	Phase transformation	Schuh et al. (2017) [80]
CrMnFeCoNi	FCC	HPT	Processing	Microstructure and texture evolution	Skrotzki et al. (2017) [81]
CoCrFeNiMn	FCC	ECAP	Processing	Microstructural features	Shahmir et al. (2017) [82]
(FeNiCoCu) _{1-x} Ti _x Al _x	FCC	HPT	Processing	Tensile properties	Zheng et al. (2017) [83]
Ti ₃₅ Zr _{27.5} Hf _{27.5} Nb ₅ Ta ₅	Orthorhombic	HPT	Processing	Lattice defects	Heczal et al. (2017) [84]
CoCrFeMnNi	FCC	HPT	Processing	Lattice defects and hardness	Heczal et al. (2017) [85]
CoCrFeMnNi	FCC + σ	HPT	Processing	Phase stability	Park et al. (2017) [86]
FeCoCrNi	FCC	HPT	Processing	Amorphization and twinning	Wu et al. (2017) [87]
Co ₂₀ Cr ₂₆ Fe ₂₀ Mn ₂₀ Ni ₁₄	HCP	HPT	Processing	Phase transformation	Moon et al. (2017) [88]
CoCrFeMnNi	FCC	HPT	Processing	Annealing effect on plastic flow	Lee et al. (2017) [89]
Al _{0.5} CoCrFeMnNi	FCC + B2	HPT	Processing	Microstructure and phase transformation	Reddy et al. (2017) [90]
TiZrNbHfTa	BCC	HPT	Processing	Thermodynamic instability	Schuh et al. (2018) [91]
Co ₂₀ Cr ₂₀ Fe ₂₀ Mn ₂₀ Ni ₂₀	FCC	HPT	Processing	Micro-scale mechanical behavior	Kawasaki et al. (2018) [92]
CoCrFeNiMn	FCC	HPT	Processing	Superplasticity	Shahmir et al. (2018) [93]
CoCrFeMnNi	FCC	Caliber Rolling	Processing	Microstructural features	Won et al. (2018) [94]
CoCrFeMnNi	FCC	HPT	Processing	Phase stability and strengthening	Shahmir et al. (2018) [95]
CoCrFeNiMn	FCC	HPT	Processing	Superplasticity	Shahmir et al. (2018) [96]
Carbon-doped CrFe ₂ NiMnV _{0.25}	FCC + Carbide	HPT	Processing	Carbon and annealing effect on hardness	Shahmir et al. (2018) [97]
HfNbTaTiZr	BCC	HPT	Processing	Lattice defects	Lukáča et al. (2018) [98]
HfNbTaTiZr	BCC	HPT	Processing	Mechanical properties	Čížek et al. (2018) [99]
CoCrFeNiNb _x	FCC	HPT	Processing	Dislocation structure	Maity et al. (2018) [100]
CoCrFeMnNi	FCC	HPT	Cryogenic Processing	Microstructure and mechanical properties	Zherebtsov et al. (2018) [101]
AlNbTiVZr _{0.5}	B2	HPT	Processing	Microstructural and hardness	Stepanov et al. (2018) [102]
Al _{0.3} CrFeCoNi	BCC + FCC	HPT	Processing	Deformation behavior	Qiang et al. (2018) [103]
CoCrFeMnNi	FCC	HPT	Synthesis	Activation energy for plastic flow	Lee et al. (2018) [104]
CoCrFeMnNi	FCC	HPT	Synthesis	Microstructure and hardness	Kilmametov et al. (2019) [105]
Hf ₂₅ Nb ₂₅ Ti ₂₅ Zr ₂₅	BCC	HPT	Processing	Microstructure and hardness	Gubicza et al. (2019) [106]
CoCrFeNi	FCC	HPT	Processing	Microstructure and hardness	Gubicza et al. (2019) [107]
CoCuFeMnNi	FCC	HPT	Monotonic and Cyclic Processing	Microstructure and hardness	Sonkusare et al. (2019) [108]
CrMnFeCoNi	FCC	HPT	Processing	Ductility	Schuh et al. (2019) [109]
CoCrFeNiMn	FCC	HPT	Processing	Nanoindentation creep behavior	Zhou et al. (2019) [110]
V ₁₀ Cr ₁₅ Mn ₅ Fe ₃₅ Co ₁₀ Ni ₂₅	FCC	HPT	Processing	Superplasticity	Nguyen et al. (2019) [111]
HfNbTaTiZr	BCC	HPT	Processing	Microstructure and mechanical properties	Málek et al. (2019) [112]
TiZrCrMnFeNi	C14 + B2	HPT	Processing	Hydrogen storage	Edalati et al. (2020) [113]

V ₁₀ Cr ₁₅ Mn ₅ Fe ₃₅ Co ₁₀ Ni ₂₅	FCC	HPT	Processing	Grain size effect on deformation mechanism	Asghari-Rad <i>et al.</i> (2020) [114]
CoCrFeNiMn	FCC	HPT	Cryogenic Processing	Microstructure and strength	Podolskiy <i>et al.</i> (2020) [115]
V ₁₀ Cr ₁₅ Mn ₅ Fe ₃₅ Co ₁₀ Ni ₂₅	FCC	HPT	Processing	Mechanical properties	Asghari-Rad <i>et al.</i> (2020) [116]
MgVTiCrFe	BCC	HPT	Processing	Hydrogen storage	de Marco <i>et al.</i> (2020) [117]
CoCuFeMnNi	FCC	HPT	Processing	Microstructure, texture and mechanical properties	Sonkusare <i>et al.</i> (2020) [118]
CoCrFeNi	FCC	HPT	Processing	Strain-rate sensitivity	Zhao <i>et al.</i> (2020) [119]
Fe ₂₀ Mn ₂₀ Ni ₂₀ Co ₂₀ Cr ₂₀	FCC	HPT	Processing	Hydrogen diffusion	Belo <i>et al.</i> (2020) [120]
Fe ₄₁ Mn ₂₅ Ni ₂₄ Co ₈ Cr ₂	FCC	Differential Rolling	Processing	Tensile properties	Jeong <i>et al.</i> (2020) [121]
CrMnFeCoNi	FCC + HCP	HPT	Processing	Microstructure, texture and strength	Skrotzki <i>et al.</i> (2020) [122]
TiAlFeCoNi	BCC + L2 ₁	HPT	Processing	Biocompatibility	Edalati <i>et al.</i> (2020) [123]
CrFeCoNi	FCC	ECAP	Processing	Microstructure	Rymer <i>et al.</i> (2020) [124]
HfNbTiZr	BCC + HCP	HPT	Processing	Thermal stability	Hung <i>et al.</i> (2020) [125]
TiZrNbHfTaO ₁₁	Monoclinic + Orthorhombic	HPT	Synthesis	Photocatalytic H ₂ production	Edalati <i>et al.</i> (2020) [126]
TiZrNbHfTaO ₆ N ₃	FCC + Monoclinic	HPT	Synthesis	Photocatalytic H ₂ production	Edalati <i>et al.</i> (2021) [127]
CoCrNiFeMn	FCC	ECAP	Processing	Low-cycle fatigue	Picak <i>et al.</i> (2021) [128]
CoCrFeNiMn	FCC + BCC	HPT	Processing	Phase transformation	Shahmir <i>et al.</i> (2021) [129]
Carbon-doped CoCrFeMnNi	FCC	HPT	Processing	Carbon effect on microstructure	Lu <i>et al.</i> (2021) [130]
Co _{17.5} Cr _{12.5} Fe ₅₅ Ni ₁₀ Mo ₅	FCC	HPT	Processing	Strengthening by precipitates and nanograins	Kwon <i>et al.</i> (2021) [131]
Fe ₄₀ Mn ₄₀ Co ₁₀ Cr ₁₀	HCP + FCC	HPT	Processing	Plasticity and non-basal slip	Chandan <i>et al.</i> (2021) [132]
CoCrFeMnNi	FCC	ECAP	Processing	Twinning and phase transformation	Picak <i>et al.</i> (2021) [133]
TiNbZrTaHf	BCC	HPT	Synthesis	Biocompatibility	González-Masís <i>et al.</i> (2021) [134]
CoCrFeNiNb _x	FCC	HPT	Processing	Strength and elasticity	Maity <i>et al.</i> (2021) [135]
Carbon-doped AlTiFeCoNi	BCC + FCC	HPT	Processing	Ultrahigh hardness and phase transformation	Edalati <i>et al.</i> (2021) [136]
AlCrFeCoNiNb	BCC + C14	HPT	Processing	Ultrahigh hardness	Edalati <i>et al.</i> (2021) [137]
CoCrFeMnNi	FCC	HPT	consolidation	Mechanical properties	Asghari-Rad <i>et al.</i> (2021) [138]
Fe ₄₀ Mn ₄₀ Co ₁₀ Cr ₁₀	FCC	HPT	Processing	Strain-induced phase transformation and plasticity	Sathiyamoorthi <i>et al.</i> (2021) [139]
(CrMnFeCo) _x Ni _{1-x}	FCC	HPT	Processing	Microstructural saturation	Keil <i>et al.</i> (2021) [140]
CoCrFeNi	FCC	HPT	Processing	Micromechanical properties	Zhao <i>et al.</i> (2021) [141]
CoCrFeMnNi-based Composite	FCC	HPT	synthesis	Microstructure and mechanical properties	Karthik <i>et al.</i> (2021) [142]
CoCrFeMnNi + HfNbTaTiZr Composite	FCC + BCC	HPT	Synthesis	Microstructure	Taheriniya <i>et al.</i> (2021) [143]
AlCrFe ₂ Ni ₂	FCC	HPT	Processing	Phase transformation	Liu <i>et al.</i> (2021) [144]
Various Materials	Review paper on synthesis of high-entropy alloys and ceramics by HPT				Edalati <i>et al.</i> (2021) [65]
CoCrFeNiMn	FCC	HPT	Processing	Micromechanical properties	Rusakova <i>et al.</i> (2021) [145]

CoCrFeNi	FCC	HPT	Processing	Annealing effect on microstructure	Hung <i>et al.</i> (2021) [146]
CoCrFeMnNi	FCC	HPT	consolidation	Microstructural features	Asghari-Rad <i>et al.</i> (2021) [147]
Various Alloys	Review paper regarding the impact of HPT on mechanical properties of high-entropy alloys				Li <i>et al.</i> (2022) [148]
Al _{0.5} CoCrFeMnNi	FCC	HPT	Processing	Superplasticity	Nguyen <i>et al.</i> (2022) [149]
CoCrFeMnNi	FCC	HPT	Processing	Corrosion resistance	Shimizu <i>et al.</i> (2022) [150]
FeCoNiCu	FCC	HPT	Processing	Mechanical properties and thermal stability	Zhang <i>et al.</i> (2022) [151]
Fe ₄₀ Mn ₄₀ Co ₁₀ Cr ₁₀	FCC	HPT	Processing	Nickel effect on microstructure	Chandan <i>et al.</i> (2022) [152]
Al _{0.7} CoCrFeNi	FCC + BCC	HPT	Synthesis	Hydrogen effect on strengthening	Gao <i>et al.</i> (2022) [153]
TiZrNbHfTaO ₆ N ₃	FCC + Monoclinic	HPT	Synthesis	CO ₂ photoreduction	Akrami <i>et al.</i> (2022) [154]
TiZrNbHfTaO ₁₁	Monoclinic + Orthorhombic	HPT	Synthesis	CO ₂ photoreduction	Akrami <i>et al.</i> (2022) [155]
CrMnFeCoNi	FCC	HPT	Processing	Mechanical properties and thermal stability	Keil <i>et al.</i> (2022) [156]
CoCrFeNi	FCC	HPT	Synthesis	Tensile properties	Son <i>et al.</i> (2022) [157]
FeNi ₂ CoMo _{0.2} V _{0.5}	FCC	HPT	Processing	Thermal stability	Liang <i>et al.</i> (2022) [158]
Al _{0.3} CoCrNi	FCC + B2 + σ	HPT	Processing	Superplasticity	Nguyen <i>et al.</i> (2022) [159]
TiZrNbTaWO ₁₂	Multiphases	HPT	Synthesis	Photocatalytic O ₂ production	Edalati <i>et al.</i> (2022) [160]
CoCrFeNi	FCC	HPT	Processing	Thermal stability	Hung <i>et al.</i> (2022) [161]
Various Alloys	Review on phase transformations of severely deformed high-entropy alloys				Straumal <i>et al.</i> (2022) [162]
AlFeCoNiCu	FCC + BCC	HPT	Processing	Lattice defects and microhardness	Edalati <i>et al.</i> (2022) [163]
MoNbTaTiVZr	BCC + BCC	HPT	Processing	Strain hardening	Duan <i>et al.</i> (2022) [164]
CrMnFeCoNi		HPT		Hydrogen embrittlement	Mohammadi <i>et al.</i> (2022) [165]
FeCoNiMn	FCC	HPT	Processing	Homogenization effect on hardness	Alijani <i>et al.</i> (2022) [166]
CrMnFeCoNi		HPT		Hydrogen embrittlement	Mohammadi <i>et al.</i> (2022) [167]
Co _{25-x} Cr ₂₅ Fe ₂₅ Ni ₂₅ C _x	FCC	HPT	Processing	Micromechanical properties	Levenets <i>et al.</i> (2022) [168]
Al _{0.1} CoCrFeNi	FCC	ECAP	Processing	Microstructure and mechanical properties	Bian <i>et al.</i> (2022) [169]

References

- [1] Azushima A, Kopp R, Korhonen A, Yang DY, Micari F, Lahoti GD, Groche P, Yanagimoto J, Tsuji N, Rosochowski A, Yanagida A. Severe plastic deformation (SPD) processes for metals. *CRIP Ann Manuf. Technol.* 2008;57:716–735. <https://doi.org/10.1016/j.cirp.2008.09.005>.
- [2] Valiev RZ, Estrin Y, Horita Z, Langdon TG, Zehetbauer MJ, Zhu YT. Producing bulk ultrafine-grained materials by severe plastic deformation: ten years later. *JOM.* 2016;68: 1216–1226. <https://doi.org/10.1007/s11837-006-0213-7>.
- [3] Segal V. Review: modes and processes of severe plastic deformation (SPD). *Materials.* 2018;11:1175. <https://doi.org/10.3390/ma11071175>.

- [4] Valiev RZ, Straumal B, Langdon TG. Using severe plastic deformation to produce nanostructured materials with superior properties. *Annu Rev Mater Res.* 2022;52:357–382. <https://doi.org/10.1146/annurev-matsci-081720-123248>.
- [5] Zehetbauer M, Grossinger R, Krenn H, Krystian M, Pippan R, Rogl P, Waitz T, Wurschum R. Bulk nanostructured functional materials by severe plastic deformation. *Adv Eng Mater.* 2010;12:692–700. <https://doi.org/10.1002/adem.201000119>.
- [6] Pippan R, Scheriau S, Taylor A, Hafok M, Hohenwarter A, Bachmaier A. Saturation of fragmentation during severe plastic deformation. *Annu Rev Mater Res.* 2010;40:319–343. <https://doi.org/10.1146/annurev-matsci-070909-104445>.
- [7] Estrin Y, Vinogradov A. Extreme grain refinement by severe plastic deformation: a wealth of challenging science. *Acta Mater.* 2013;61:782–817. <https://doi.org/10.1016/j.actamat.2012.10.038>.
- [8] Starink MJ, Cheng XC, Yang S. Hardening of pure metals by high-pressure torsion: A physically based model employing volume-averaged defect evolutions. *Acta Mater.* 2013;61:183–192. <https://doi.org/10.1016/j.actamat.2012.09.048>.
- [9] Edalati K, Bachmaier A, Beloshenko VA, Beygelzimer Y, Blank VD, Botta WJ, Bryła K, Čížek J, Divinski S, Enikeev NA, Estrin Y, Faraji G, Figueiredo RB, Fuji M, Furuta T, Grosdidier T, Gubicza J, Hohenwarter A, Horita Z, Huot J, Ikoma Y, Janeček M, Kawasaki M, Král P, Kuramoto S, Langdon TG, Leiva DR, Levitas VI, Mazilkin A, Mito M, Miyamoto H, Nishizaki T, Pippan R, Popov VV, Popova EN, Purcek G, Renk O, Révész Á, Sauvage X, Sklenicka V, Skrotzki W, Straumal BB, Suwas S, Toth LS, Tsuji N, Valiev RZ, Wilde G, Zehetbauer MJ, Zhu X. Nanomaterials by severe plastic deformation: review of historical developments and recent advances. *Mater Res Lett.* 2022;10:163–256. <https://doi.org/10.1080/21663831.2022.2029779>.
- [10] Bridgman PW. Effects of high shearing stress combined with high hydrostatic pressure. *Phys Rev.* 1935;48:825–847. <https://doi.org/10.1103/PhysRev.48.825>.
- [11] Edalati K, Horita Z. A review on high-pressure torsion (HPT) from 1935 to 1988. *Mater Sci Eng A.* 2016;652:325–352. <https://doi.org/10.1016/j.msea.2015.11.074>.
- [12] Bryła K, Edalati K. Historical studies by Polish scientist on ultrafine-grained materials by severe plastic deformation. *Mater Trans.* 2019;60:1553–1560.
- [13] Segal VM, Reznikov VI, Drobysheskiy AE, Kopylov VI. Plastic working of metals by simple shear. *Russ Metall.* 1981;1:99–105. <https://doi.org/10.2320/matertrans.MF201921>.
- [14] Valiev RZ, Kaibyshev OA, Kuznetsov RI, Musalimov RS, Tsenev NK. Low-temperature superplasticity of metallic materials. *Dokl Akad Nauk SSSR.* 1988;301:864–866.
- [15] Edalati K, Horita Z. Special issue on severe plastic deformation for nanomaterials with advanced functionality. *Mater Trans.* 2019;60:1103. <https://doi.org/10.2320/matertrans.MPR2019904>.
- [16] Horita Z, Edalati K. Severe plastic deformation for nanostructure controls. *Mater Trans.* 2020;61:2241–2247. <https://doi.org/10.2320/matertrans.MT-M2020134>.
- [17] Pereira PHR, Figueiredo RB. Finite element modelling of high-pressure torsion: an overview. *Mater Trans.* 2019;60:1139–1150. <https://doi.org/10.2320/matertrans.MF201906>.
- [18] Renk O, Pippan R. Saturation of grain refinement during severe plastic deformation of single phase materials: reconsiderations, current status and open questions. *Mater Trans.* 2019;60:1270–1282. <https://doi.org/10.2320/matertrans.MF201918>.

- [19] Levitas VI. High-pressure phase transformations under severe plastic deformation by torsion in rotational anvils. *Mater Trans.* 2019;60:1294–1301. <https://doi.org/10.2320/matertrans.MF201923>.
- [20] Tsuji N, Gholizadeh R, Ueji R, Kamikawa N, Zhao L, Tian Y, Bai Y, Shibata A. Formation mechanism of ultrafine grained microstructures: various possibilities for fabricating bulk nanostructured metals and alloys. *Mater Trans.* 2019;60:1518–1532. <https://doi.org/10.2320/matertrans.MF201936>.
- [21] Popov VV, Popova EN. Behavior of Nb and CuNb composites under severe plastic deformation and annealing. *Mater Trans.* 2019;60:1209–1220. <https://doi.org/10.2320/matertrans.MF201913>.
- [22] Skrotzki W. Deformation heterogeneities in equal channel angular pressing. *Mater Trans.* 2019;60:1331–1343. <https://doi.org/10.2320/matertrans.MF201926>.
- [23] Miura H, Iwama Y, Kobayashi M. Comparisons of microstructures and mechanical properties of heterogeneous nano-structure induced by heavy cold rolling and ultrafine-grained structure by multi-directional forging of CuAl alloy. *Mater Trans.* 2019;60:1111–1115. <https://doi.org/10.2320/matertrans.MF201904>.
- [24] Faraji G, Torabzadeh H. An overview on the continuous severe plastic deformation methods. *Mater Trans.* 2019;60:1316–1330. <https://doi.org/10.2320/matertrans.MF201905>.
- [25] Masuda T, Horita Z. Grain refinement of AZ31 and AZ61 Mg alloys through room temperature processing by up-scaled high-pressure torsion. *Mater Trans.* 2019;60:1104–1110. <https://doi.org/10.2320/matertrans.M2018308>.
- [26] Toth LS, Chen C, Pougis A, Arzaghi M, Fundenberger JJ, Massion R, Suwas S. High pressure tube twisting for producing ultra fine grained materials: a review. *Mater Trans.* 2019;60:1177–1191. <https://doi.org/10.2320/matertrans.MF201910>.
- [27] Blank VD, Popov MY, Kulnitskiy BA. The effect of severe plastic deformations on phase transitions and structure of solids. *Mater Trans.* 2019;60:1500–1505. <https://doi.org/10.2320/matertrans.MF201942>.
- [28] Grosdidier T, Novelli M. Recent developments in the application of surface mechanical attrition treatments for improved gradient structures: processing parameters and surface reactivity. *Mater Trans.* 2019;60:1344–1355. <https://doi.org/10.2320/matertrans.MF201929>.
- [29] Yang X, Pan H, Zhang J, Gao H, Shu B, Gong Y, Zhu X. Progress in mechanical properties of gradient structured metallic materials induced by surface mechanical attrition treatment. *Mater Trans.* 2019;60:1543–1552. <https://doi.org/10.2320/matertrans.MF201911>.
- [30] Ikoma Y. Severe plastic deformation of semiconductor materials using high-pressure torsion. *Mater Trans.* 2019;60:1168–1176. <https://doi.org/10.2320/matertrans.MF201907>.
- [31] Beloshenko V, Vozniak I, Beygelzimer Y, Estrin Y, Kulagin R. Severe plastic deformation of polymers. *Mater Trans.* 2019;60:1192–1202. <https://doi.org/10.2320/matertrans.MF201912>.
- [32] Razavi-Khosroshahi H, Fuji M. Development of metal oxide high-pressure phases for photocatalytic properties by severe plastic deformation. *Mater Trans.* 2019;60:1203–1208. <https://doi.org/10.2320/matertrans.MF201916>.
- [33] Révész Á, Kovács Z. Severe plastic deformation of amorphous alloys. *Mater Trans.* 2019;60:1283–1293. <https://doi.org/10.2320/matertrans.MF201917>.
- [34] Sauvage X, Duchaussoy A, Zaher G. Strain induced segregations in severely deformed materials. *Mater Trans.* 2019;60:1151–1158. <https://doi.org/10.2320/matertrans.MF201919>.

- [35] Gubicza J. Lattice defects and their influence on the mechanical properties of bulk materials processed by severe plastic deformation. *Mater Trans.* 2019;60:1230–1242. <https://doi.org/10.2320/matertrans.MF201909>.
- [36] Suwas S, Mondal S. Texture evolution in severe plastic deformation processes. *Mater Trans.* 2019;60:1457–1471. <https://doi.org/10.2320/matertrans.MF201933>.
- [37] Wilde G, Divinski S. Grain boundaries and diffusion phenomena in severely deformed materials. *Mater Trans.* 2019;60:1302–1315. <https://doi.org/10.2320/matertrans.MF201934>.
- [38] Čížek J, Janeček M, Vlasák T, Smola B, Melikhova O, Islamgaliev RK, Dobatkin SV. The development of vacancies during severe plastic deformation. *Mater Trans.* 2019;60:1533–1542. <https://doi.org/10.2320/matertrans.MF201937>.
- [39] Han JK, Jang, Langdon TG, Kawasaki M. Bulk-state reactions and improving the mechanical properties of metals through high-pressure torsion. *Mater Trans.* 2019;60:1131–1138. <https://doi.org/10.2320/matertrans.MF201908>.
- [40] Edalati K. Metallurgical alchemy by ultra-severe plastic deformation via high-pressure torsion process. *Mater Trans.* 2019;60:1221–1229. <https://doi.org/10.2320/matertrans.MF201914>.
- [41] Bachmaier A, Pippan R. High-pressure torsion deformation induced phase transformations and formations: new material combinations and advanced properties. *Mater Trans.* 2019;60:1256–1269. <https://doi.org/10.2320/matertrans.MF201930>.
- [42] Mazilkin A, Straumal B, Kilmametov A, Straumal P, Baretzky B. Phase transformations induced by severe plastic deformation. *Mater Trans.* 2019;60:1489–1499. <https://doi.org/10.2320/matertrans.MF201938>.
- [43] Kuramoto S, Furuta. Severe plastic deformation to achieve high strength and high ductility in FeNi based alloys with lattice softening. *Mater Trans.* 2019;60:1116–1122. <https://doi.org/10.2320/matertrans.MF201920>.
- [44] Kawasaki M, Langdon TG. The contribution of severe plastic deformation to research on superplasticity. *Mater Trans.* 2019;60:1123–1130. <https://doi.org/10.2320/matertrans.MF201915>.
- [45] Demirtas M, Purcek G. Room temperature superplasticity in fine/ultrafine grained materials subjected to severe plastic deformation. *Mater Trans.* 2019;60:1159–1167. <https://doi.org/10.2320/matertrans.MF201922>.
- [46] Kunimine T, Watanabe M. A comparative study of hardness in nanostructured Cu-Zn, Cu-Si and Cu-Ni solid-solution alloys processed by severe plastic deformation. *Mater Trans.* 2019;60:1484–1488. <https://doi.org/10.2320/matertrans.MF201944>.
- [47] Kral P, Dvorak J, Sklenicka V, Langdon TG. The characteristics of creep in metallic materials processed by severe plastic deformation. *Mater Trans.* 2019;60:1506–1517. <https://doi.org/10.2320/matertrans.MF201924>.
- [48] Moreno-Valle EC, Pachla W, Kulczyk M, Sabirov I, Hohenwarter A. Anisotropy of tensile and fracture behavior of pure titanium after hydrostatic extrusion. *Mater Trans.* 2019;60:2160–2167. <https://doi.org/10.2320/matertrans.MF201928>.
- [49] Nishizaki T, Edalati K, Lee S, Horita Z, Akune T, Nojima T, Iguchi S, Sasaki T. Critical temperature in bulk ultrafine-grained superconductors of Nb, V, and Ta processed by high-pressure torsion. *Mater Trans.* 2019;60:1367–1376. <https://doi.org/10.2320/matertrans.MF201940>.

- [50] Miyamoto H, Yuasa M, Rifai M, Fujiwara H. Corrosion behavior of severely deformed pure and single-phase materials. *Mater Trans.* 2019;60:1243–1255. <https://doi.org/10.2320/matertrans.MF201935>.
- [51] Valiev RZ, Parfenov EV, Parfenova LV. Developing nanostructured metals for manufacturing of medical implants with improved design and biofunctionality. *Mater Trans.* 2019; 60:1356–1366. <https://doi.org/10.2320/matertrans.MF201943>.
- [52] Mito M, Shigeoka S, Kondo H, Noumi N, Kitamura Y, Irie K, Nakamura K, Takagi S, Deguchi H, Tajiri T, Ishizuka M, Nishizaki T, Edalati K, Horita Z. Hydrostatic compression effects on fifth-group element superconductors V, Nb, and Ta subjected to high-pressure torsion. *Mater Trans.* 2019;60:1472–1483. <https://doi.org/10.2320/matertrans.MF201932>.
- [53] Leiva DR, AM Jorge, Jr., Ishikawa TT, Botta WJ. Hydrogen storage in Mg and Mg-based alloys and composites processed by severe plastic deformation. *Mater Trans.* 2019;60: 1561–1570. <https://doi.org/10.2320/matertrans.MF201927>.
- [54] Huot J, Tournant M. Effect of cold rolling on metal hydrides. *Mater Trans.* 2019;60:1571–1576. <https://doi.org/10.2320/matertrans.MF201939>.
- [55] Enikeev NA, Shamardin VK, Radiguet B. Radiation tolerance of ultrafine-grained materials fabricated by severe plastic deformation. *Mater Trans.* 2019;60:1723–1731. <https://doi.org/10.2320/matertrans.MF201931>.
- [56] Rogl G, Zehetbauer MJ, Rogl PF. The effect of severe plastic deformation on thermoelectric performance of skutterudites, half-Heuslers and Bi-tellurides. *Mater Trans.* 2019;60:2071–2085. <https://doi.org/10.2320/matertrans.MF201941>.
- [57] Zhang Y, Zuo TT, Tang Z, Gao MC, Dahmen KA, Liaw PK, Lu ZP. Microstructures and properties of high-entropy alloys. *Prog Mater Sci.* 2014;61:1–93. <https://doi.org/10.1016/j.pmatsci.2013.10.001>.
- [58] George EP, Raabe D, Ritchie RO. High-entropy alloys. *Nat Rev Mater.* 2019;4:515–534. <https://doi.org/10.1038/s41578-019-0121-4>.
- [59] Inui H, Kishida K, Chen Z. Recent progress in our understanding of phase stability, atomic structures and mechanical and functional properties of high-entropy alloys. *Mater Trans.* 2022;63:394–401. <https://doi.org/10.2320/matertrans.MT-M2021234>.
- [60] Harrington TJ, Gild J, Sarker P, Toher C, Rost CM, Dippo OF, McElfresh C, Kaufmann K, Marin E, Borowski L, Hopkins PE, Luo J, Curtarolo S, Brenner DW, Vecchio KS. Phase stability and mechanical properties of novel high entropy transition metal carbides. *Acta Mater.* 2019;166:271–280. <https://doi.org/10.1016/j.actamat.2018.12.054>.
- [61] Oses C, Toher C, Curtarolo S. High-entropy ceramics. *Nat Rev Mater.* 2020;5:295–309. <https://doi.org/10.1038/s41578-019-0170-8>.
- [62] Akrami S, Edalati P, Fuji M, Edalati K. High-entropy ceramics: review of principles, production and applications. *Mater Sci Eng R.* 2021;146:100644. <https://doi.org/10.1016/j.mser.2021.100644>.
- [63] Yeh JW, Chen SK, Lin SJ, Gan JY, Chin TS, Shun TT, Tsau CH, Chang SY. Nanostructured high-entropy alloys with multiple principal elements: novel alloy design concepts and outcomes. *Adv Eng Mater.* 2004;6:299–303. <https://doi.org/10.1002/adem.200300567>.
- [64] Cantor B, Chang I, Knight P, Vincent A. Microstructural development in equiatomic multicomponent alloys. *Mater Sci Eng A.* 2004;375:213–218. <https://doi.org/10.1016/j.msea.2003.10.257>.

- [65] Edalati K, Li HW, Kilmametov A, Floriano R, Borchers C. High-pressure torsion for synthesis of high-entropy alloys. *Metals*. 2021;11:1263. <https://doi.org/10.3390/met11081263>.
- [66] Kuznetsov AV, Shaysultanov DG, Stepanov ND, Salishchev GA, Senkov ON. Superplasticity of AlCoCrCuFeNi high entropy alloy. *Mater Sci Forum*. 2013;735:146–151. <https://doi.org/10.4028/www.scientific.net/MSF.735.146>.
- [67] Hammond VH, Atwater MA, Darling KA, Nguyen HQ, Kecskes LJ. Equal-channel angular extrusion of a low-density high-entropy alloy produced by high-energy cryogenic mechanical alloying. *JOM*. 2014;66:2021–2029. <https://doi.org/10.1007/s11837-014-1113-x>.
- [68] Schuh B, Mendez-Martin F, Völker B, George EP, Clemens H, Pippan R, Hohenwarter A. Mechanical properties, microstructure and thermal stability of a nanocrystalline CoCrFeMnNi high-entropy alloy after severe plastic deformation. *Acta Mater*. 2015;96:258–268. <https://doi.org/10.1016/j.actamat.2015.06.025>.
- [69] Tang QH, Huang Y, Huang YY, Liao XZ, Langdon TG, Dai PQ. Hardening of an Al_{0.3}CoCrFeNi high entropy alloy via high-pressure torsion and thermal annealing. *Mater Lett*. 2015;151:126–129. <https://doi.org/10.1016/j.matlet.2015.03.066>.
- [70] Lee DH, Choi IC, Seok MY, He J, Lu Z, Suh JY, Kawasaki M, Langdon TG, Jang J. Nanomechanical behavior and structural stability of a nanocrystalline CoCrFeNiMn high-entropy alloy processed by high-pressure torsion. *J Mater Res*. 2015;30:2804–2815. <https://doi.org/10.1557/jmr.2015.239>.
- [71] Tang QH, Liao XZ, Dai P. Microstructure evolution of Al_{0.3}CoCrFeNi high-entropy alloy during high-pressure torsion. *J Mater Eng*. 2015;43:45–51. <https://doi.org/10.11868/j.issn.1001-4381.2015.12.008>.
- [72] Yu PF, Cheng H, Zhang LJ, Zhang H, Jing Q, Ma MZ, Liaw PK, Li G, Liu RP. Effects of high pressure torsion on microstructures and properties of an Al_{0.1}CoCrFeNi high-entropy alloy. *Mater Sci Eng A*. 2016;655:283–291. <https://doi.org/10.1016/j.msea.2015.12.085>.
- [73] Lee DH, Seok MY, Zhao Y, Choi IC, He J, Lu Z, Suh JY, Ramamurty U, Kawasaki M, TG Langdon, Jang J. Spherical nanoindentation creep behavior of nanocrystalline and coarse-grained CoCrFeMnNi high-entropy alloys. *Acta Mater*. 2016;109:314–322. <https://doi.org/10.1016/j.actamat.2016.02.049>.
- [74] Tang QH, Huang Y, Cheng H, Liao XZ, Langdon TG, Dai PQ. The effect of grain size on the annealing-induced phase transformation in an Al_{0.3}CoCrFeNi high entropy alloy. *Mater Des*. 2016;105:381–385. <https://doi.org/10.1016/j.matdes.2016.05.079>.
- [75] Shahmir H, He J, Lu Z, Kawasaki M, Langdon TG. Effect of annealing on mechanical properties of a nanocrystalline CoCrFeNiMn high-entropy alloy processed by high-pressure torsion. *Mater Sci Eng A*. 2016;676:294–303. <https://doi.org/10.1016/j.msea.2016.08.118>.
- [76] Yuan H, Tsai MH, Sha G, Liu F, Horita Z, Zhu Y, Wang JT. Atomic-scale homogenization in an fcc-based high-entropy alloy via severe plastic deformation. *J Alloys Compd*. 2016;686:15–23. <https://doi.org/10.1016/j.jallcom.2016.05.337>.
- [77] Heczal A, Lilensten L, Bourgon J, Perrière L, Couzinié JP, Guillot I, Dirras G, Huang Y, Langdon TG, Gubicza J. Influence of high-pressure torsion on the microstructure and the hardness of a Ti-rich high-entropy alloy. *Mater Sci Forum* 2017;879:732–737. <https://doi.org/10.4028/www.scientific.net/MSF.879.732>.

- [78] Maier-Kiener V, Schuh B, George EP, Clemens H, Hohenwarter A. Nanoindentation testing as a powerful screening tool for assessing phase stability of nanocrystalline high-entropy alloys. *Mater Des.* 2017;115:479–485. <https://doi.org/10.1016/j.matdes.2016.11.055>.
- [79] Shahmir H, He J, Lu Z, Kawasaki M, Langdon TG. Evidence for superplasticity in a CoCrFeNiMn high-entropy alloy processed by high-pressure torsion. *Mater Sci Eng A.* 2017;685:342–348. <https://doi.org/10.1016/j.msea.2017.01.016>.
- [80] Schuh B, Völker B, Maier-Kiener V, Todt J, Li J, Hohenwarter A. Phase decomposition of a single-phase AlTiVNb high-entropy alloy after severe plastic deformation and annealing. *Adv Eng Mater.* 2017;19:1600674. <https://doi.org/10.1002/adem.201600674>.
- [81] Skrotzki W, Pukenas A, Joni B, Odor E, Ungar T, Hohenwarter A, Pippin R, George EP. Microstructure and texture evolution during severe plastic deformation of CrMnFeCoNi high-entropy alloy. *IOP Conf Ser: Mater Sci Eng.* 2017;194:012028. <https://doi.org/10.1088/1757-899X/194/1/012028>.
- [82] Shahmir H, Mousavi T, He J, Lu Z, Kawasaki M, Langdon TG. Microstructure and properties of a CoCrFeNiMn high-entropy alloy processed by equal-channel angular pressing. *Mater Sci Eng A.* 2017;705:411–419. <https://doi.org/10.1016/j.msea.2017.08.083>.
- [83] Zheng R, Chen J, Xiao W, Ma C. Microstructure and tensile properties of nanocrystalline (FeNiCoCu)_{1-x}Ti_xAl_x high entropy alloys processed by high pressure torsion. *Intermetallics.* 2016;74:38–45. <https://doi.org/10.1016/j.intermet.2016.05.008>.
- [84] Heczal A, Huang Y, Langdon TG, Gubicza J. Investigation of lattice defects in a plastically deformed high-entropy alloy. *Mater Sci Forum.* 2017;885:74–79. <https://doi.org/10.4028/www.scientific.net/MSF.885.74>.
- [85] Heczal A, Kawasaki M, Lábár JL, Jang J, Langdon TG, Gubicza J. Defect structure and hardness in nanocrystalline CoCrFeMnNi high-entropy alloy processed by high-pressure torsion. *J Alloys Compd.* 2017;711:143–154. <https://doi.org/10.1016/j.jallcom.2017.03.352>.
- [86] Park N, Lee BJ, Tsuji N. The phase stability of equiatomic CoCrFeMnNi high-entropy alloy: comparison between experiment and calculation results. *J Alloys Compd.* 2017;719:189–193. <https://doi.org/10.1016/j.jallcom.2017.05.175>.
- [87] Wu W, Ni S, Liu Y, Liu B, Song M. Amorphization at twin-twin intersected region in FeCoCrNi high-entropy alloy subjected to high-pressure torsion. *Mater Charact.* 2017;127:111–115. <https://doi.org/10.1016/j.matchar.2017.02.027>.
- [88] Moon J, Qi Y, Tabachnikova E, Estrin Y, Choi WM, Joo SH, Lee BJ, Podolskiy A, Tikhonovsky M, Kim HS. Deformation-induced phase transformation of Co₂₀Cr₂₆Fe₂₀Mn₂₀Ni₁₄ high-entropy alloy during high-pressure torsion at 77 K. *Mater Lett.* 2017;202:86–88. <https://doi.org/10.1016/j.matlet.2017.05.065>.
- [89] Lee DH, Lee JA, Zhao Y, Lu Z, Suh JY, Kim JY, Ramamurty, Kawasaki M, Langdon TG, Jang J. Annealing effect on plastic flow in nanocrystalline CoCrFeMnNi high-entropy alloy: a nanomechanical analysis. *Acta Mater.* 2017;140:443–451. <https://doi.org/10.1016/j.actamat.2017.08.057>.
- [90] Reddy TS, Wani IS, Bhattacharjee T, Reddy SR, Saha R, Bhattacharjee PP. Severe plastic deformation driven nanostructure and phase evolution in a Al_{0.5}CoCrFeMnNi dual phase

- high entropy alloy. *Intermetallics*. 2017;91:150–157. <https://doi.org/10.1016/j.intermet.2017.09.002>.
- [91] Schuh B, Völker B, Todt J, Schell N, Perrière L, Li J, Couzinié JP, Hohenwarter A. Thermodynamic instability of a nanocrystalline, single-phase TiZrNbHfTa alloy and its impact on the mechanical properties, *Acta Mater*. 2018;142:201–212. <https://doi.org/10.1016/j.actamat.2017.09.035>.
- [92] Kawasaki M, Han JK, Lee DH, Jang Jae-II, Langdon TG. Micro-scale mechanical behavior of ultrafine-grained materials processed by high-pressure torsion. *Mater Sci Forum*. 2018;941:1495–1500. <https://doi.org/10.4028/www.scientific.net/MSF.941.1495>.
- [93] Shahmir H, Kawasaki M, Langdon TG. Developing superplasticity in high-entropy alloys processed by severe plastic deformation. *Mater Sci Forum*. 2018;941:1059–1064. <https://doi.org/10.4028/www.scientific.net/MSF.941.1059>.
- [94] Won JW, Lee S, Park SH, Kang M, Lim KR, Park CH, Na YS. Ultrafine-grained CoCrFeMnNi high-entropy alloy produced by cryogenic multi-pass caliber rolling. *J Alloys Compd*. 2018;742:290–295. <https://doi.org/10.1016/j.jallcom.2018.01.313>.
- [95] Shahmir H, Nili-Ahmadabadi M, Shafiee A, Andrzejczuk M, Lewandowska M, Langdon TG. Effect of Ti on phase stability and strengthening mechanisms of a nanocrystalline CoCrFeMnNi high-entropy alloy. *Mater Sci Eng A*. 2018;725:196–206. <https://doi.org/10.1016/j.msea.2018.04.014>.
- [96] Shahmir H, Nili-Ahmadabadi M, Shafiee A, Langdon TG. Effect of a minor titanium addition on the superplastic properties of a CoCrFeNiMn high-entropy alloy processed by high-pressure torsion. *Mater Sci Eng A*. 2018;718:468–476. <https://doi.org/10.1016/j.msea.2018.02.002>.
- [97] Shahmir H, Tabachnikova E, Podolskiy A, Tikhonovsky M, Langdon TG. Effect of carbon content and annealing on structure and hardness of CrFe₂NiMnV_{0.25} high-entropy alloys processed by high-pressure torsion. *J Mater Sci*. 2018;53:11813–11822. <https://doi.org/10.1007/s10853-018-2456-4>.
- [98] Lukáča F, Dudr M, Čížek J, Harcuba P, Vlasák T, Janeček M, Kuriplach J, Moon J, Kim, J. Zýka HS, Málek J. Defects in high entropy alloy HfNbTaTiZr prepared by high pressure torsion. *Acta Phys Pol A*. 2018;134:891–894. <http://doi.org/10.12693/APhysPolA.134.891>.
- [99] Čížek J, Haušil P, Cieslar M, Melikhova O, Vlasák T, Janeček M, Král R, Harcuba P, LukáčF, Zýka J, Málek J, Moon J, Kim HS. Strength enhancement of high entropy alloy HfNbTaTiZr by severe plastic deformation. *J Alloys Compd*. 2018;768:924–937. <https://doi.org/10.1016/j.jallcom.2018.07.319>.
- [100] Maity T, Prashanth KG, Balci Ö, Kim JT, Schöberl T, Wang Z, Eckert J. Influence of severe straining and strain rate on the evolution of dislocation structures during micro-/nanoindentation in high entropy lamellar eutectics. *Int J Plast*. 2018;109:121–136. <https://doi.org/10.1016/j.ijplas.2018.05.012>.
- [101] Zharebtsov S, Stepanov N, Ivanisenko Y, Shaysultanov D, Yurchenko N, Klimova M, Salishchev G. Evolution of microstructure and mechanical properties of a CoCrFeMnNi high-entropy alloy during high-pressure torsion at room and cryogenic temperatures. *Metals*. 2018;8:123. <https://doi.org/10.3390/met8020123>.

- [102] Stepanov ND, Yurchenko NY, Gridneva AO, Zharebtsov SV, Ivanisenko YV, Salishchev GA. Structure and hardness of B2 ordered refractory AlNbTiVZr_{0.5} high entropy alloy after high-pressure torsion. *Mater Sci Eng A*. 2018;716:308–315. <https://doi.org/10.1016/j.msea.2018.01.061>.
- [103] Qiang J, Tsuchiya K, Diao H, Liaw PK. Vanishing of room-temperature slip avalanches in a face-centered-cubic high-entropy alloy by ultrafine grain formation. *Scr Mater*. 2018;155:99–103. <https://doi.org/10.1016/j.scriptamat.2018.06.034>.
- [104] Lee DH, Choi IC, Yang G, Lu Z, Kawasaki M, Ramamurty U, Schwaiger R, Jang J. Activation energy for plastic flow in nanocrystalline CoCrFeMnNi high-entropy alloy: a high temperature nanoindentation study. *Scr Mater*. 2018;156:129–133. <https://doi.org/10.1016/j.scriptamat.2018.07.014>.
- [105] Kilmametov A, Kulagin R, Mazilkin A, Seils S, Boll T, Heilmaier M, Hahn H. High-pressure torsion driven mechanical alloying of CoCrFeMnNi high entropy alloy. *Scr Mater*. 2019;158:29–33. <https://doi.org/10.1016/j.scriptamat.2018.08.031>.
- [106] Gubicza J, Heczal A, Kawasaki M, Han JK, Zhao Y, Xue Y, Huang S, Lábár JL. Evolution of microstructure and hardness in Hf₂₅Nb₂₅Ti₂₅Zr₂₅ high-entropy alloy during high-pressure torsion. *J Alloys Compd*. 2019;788:318–328. <https://doi.org/10.1016/j.jallcom.2019.02.220>.
- [107] Gubicza J, Hung PT, Kawasaki M, Han JK, Zhao Y, Xue Y, Lábár JL. Influence of severe plastic deformation on the microstructure and hardness of a CoCrFeNi high-entropy alloy: A comparison with CoCrFeNiMn. *Mater Charact*. 2019;154:304–314. <https://doi.org/10.1016/j.matchar.2019.06.015>.
- [108] Sonkusare R, Khandelwal N, Ghosh P, Biswas K, Gurao NP. A comparative study on the evolution of microstructure and hardness during monotonic and cyclic high pressure torsion of CoCuFeMnNi high entropy alloy. *J Mater Res*. 2019;34:732–743. <https://doi.org/10.1557/jmr.2018.479>.
- [109] Schuh B, Pippan R, Hohenwarter A. Tailoring bimodal grain size structures in nanocrystalline compositionally complex alloys to improve ductility. *Mater Sci Eng A*. 2019;748:379–385. <https://doi.org/10.1016/j.msea.2019.01.073>.
- [110] Zhou PF, Xiao DH, Li G, Song M. Nanoindentation creep behavior of CoCrFeNiMn high-entropy alloy under different high-pressure torsion deformations. *J Mater Eng Perform*. 2019;28:2620–2629. <https://doi.org/10.1007/s11665-019-04092-1>.
- [111] Nguyen NTC, Moon J, Sathiyamoorthi P, Asghari-Rad P, Kim GH, Lee CS, Kim HS. Superplasticity of V₁₀Cr₁₅Mn₅Fe₃₅Co₁₀Ni₂₅ high-entropy alloy processed using high-pressure torsion. *Mater Sci Eng A*. 2019;764:138198. <https://doi.org/10.1016/j.msea.2019.138198>.
- [112] Málek J, Zýka J, Lukáč F, Vilémová M, Vlasák T, Čížek J, Melikhova O, Macháček A, Kim HS. The effect of processing route on properties of HfNbTaTiZr high entropy alloy. *Materials*. 2019;12:4022. <https://doi.org/10.3390/ma12234022>.
- [113] Edalati P, Floriano R, Mohammadi A, Li Y, Zepon G, Li HW, Edalati K. Reversible room temperature hydrogen storage in high-entropy alloy TiZrCrMnFeNi. *Scr Mater*. 2020;178:387–390. <https://doi.org/10.1016/j.scriptamat.2019.12.009>.

- [114] Asghari-Rad P, Sathiyamoorthi , Bae JW, Shahmir H, Zargaran A, Kim HS. Effect of initial grain size on deformation mechanism during high-pressure torsion in $V_{10}Cr_{15}Mn_5Fe_{35}Co_{10}Ni_{25}$ high-entropy alloy. *Adv Eng Mater.* 2020;22:1900587. <https://doi.org/10.1002/adem.201900587>.
- [115] Podolskiy AV, Shapovalov YO, Tabachnikova ED, Tortika AS, Tikhonovsky MA, Joni B, Ódor E, Ungar T, Maier S, Rentenberger C, Zehetbauer MJ, Schafner E. Anomalous evolution of strength and microstructure of high-entropy alloy CoCrFeNiMn after high-pressure torsion at 300 and 77 K. *Adv Eng Mater.* 2020;22:1900752. <https://doi.org/10.1002/adem.201900752>.
- [116] Asghari-Rad P, Sathiyamoorthi P, Nguyen NTC, Bae J, Shahmir H, Kim HS. Fine-tuning of mechanical properties in $V_{10}Cr_{15}Mn_5Fe_{35}Co_{10}Ni_{25}$ high-entropy alloy through high-pressure torsion and annealing. *Mater Sci Eng A.* 2020;771:138604. <https://doi.org/10.1016/j.msea.2019.138604>.
- [117] de Marco MO, Li Y, Li HW, Edalati K, Floriano R. Mechanical synthesis and hydrogen storage characterization of MgVCr and MgVTiCrFe high-entropy alloy. *Adv Eng Mater.* 2020;22:1901079. <https://doi.org/10.1002/adem.201901079>.
- [118] Sonkusare R, Biswas K, Al- Hamdany N, Brokmeier HG, Kalsar R, Schell N, NP Gurao. A critical evaluation of microstructure-texture-mechanical behavior heterogeneity in high pressure torsion processed CoCuFeMnNi high entropy alloy. *Mater Sci Eng A.* 2020;782:139187. <https://doi.org/10.1016/j.msea.2020.139187>.
- [119] Zhao Y, Wang X, Cao T, Han JK, Kawasaki M, Jang J, Han HN, Ramamurty U, Wang L, Xue Y. Effect of grain size on the strain rate sensitivity of CoCrFeNi high-entropy alloy. *Mater Sci Eng A.* 2020;782:139281. <https://doi.org/10.1016/j.msea.2020.139281>.
- [120] Belo JS, Marques SC, Castilho AV, de Oliveira LM, Simão RA, dos Santos DS. Hydrogen diffusivity and interaction with $Fe_{20}Mn_{20}Ni_{20}Co_{20}Cr_{20}$ and $Fe_{22}Mn_{40}Ni_{30}Co_6Cr_2$ high-entropy alloys. *J Alloys Compd.* 2020;815:152314. <https://doi.org/10.1016/j.jallcom.2019.152314>.
- [121] Jeong HT, Kim WJ. Grain size and temperature effect on the tensile behavior and deformation mechanisms of non-equiatomic $Fe_{41}Mn_{25}Ni_{24}Co_8Cr_2$ high entropy alloy. *J Mater Sci Technol.* 2020;42:190–202. <https://doi.org/10.1016/j.jmst.2019.09.034>.
- [122] Skrotzki W, Pukenas A, Odor E, Joni B, Ungar T, Völker B, Hohenwarter A, Pippan R, EP George. Microstructure, texture, and strength development during high-pressure torsion of CrMnFeCoNi high-entropy alloy. *Crystals.* 2020;10:336. <https://doi.org/10.3390/cryst10040336>.
- [123] Edalati P, Floriano R, Tang Y, Mohammadi A, Pereira KD, Luchessi AD, Edalati K. Ultrahigh hardness and biocompatibility of high-entropy alloy TiAlFeCoNi processed by high-pressure torsion. *Mater Sci Eng C.* 2020;112:110908. <https://doi.org/10.1016/j.msec.2020.110908>.
- [124] Rymer LM, Lindner T, Frint P, Löbel M, Lampke T. Designing (ultra) fine-grained high-entropy alloys by spark plasma sintering and equal-channel angular pressing. *Crystals.* 2020;10:1157. <https://doi.org/10.3390/cryst10121157>.

- [125] Hung PT, Kawasaki M, Han JK, Lábár JL, Gubicza J. Thermal stability of a nanocrystalline HfNbTiZr multi-principal element alloy processed by high-pressure torsion. *Mater Charact.* 2020;168:110550. <https://doi.org/10.1016/j.matchar.2020.110550>.
- [126] Edalati P, Wang Q, Razavi-Khosroshahi H, Fuji M, Ishihara T, Edalati K. Photocatalytic hydrogen evolution on a high-entropy oxide. *J Mater Chem A.* 2020;8:3814–3821. <https://doi.org/10.1039/C9TA12846H>.
- [127] Edalati P, Shen XF, Watanabe M, Ishihara T, Arita M, Fuji M, Edalati K. High-entropy oxynitride as low-bandgap and stable photocatalyst for hydrogen production. *J Mater Chem A.* 2021;9:15076–15086. <https://doi.org/10.1039/D1TA03861C>.
- [128] Picak S, Wegener T, Sajadifar SV, Sobrero C, Richter J, Kim H, Niendorf T, Karaman I. On the low-cycle fatigue response of CoCrNiFeMn high entropy alloy with ultra-fine grain structure. *Acta Mater.* 2021;205:116540. <https://doi.org/10.1016/j.actamat.2020.116540>.
- [129] Shahmir H, Asghari-Rad P, Mehranpour MS, Forghani F, Kim HS, Nili-Ahmadabad M. Evidence of FCC to HCP and BCC-martensitic transformations in a CoCrFeNiMn high-entropy alloy by severe plastic deformation. *Mater Sci Eng A.* 2021;807:140875. <https://doi.org/10.1016/j.msea.2021.140875>.
- [130] Lu Y, Mazilkin A, Boll T, Stepanov N, Zharebtzov S, Salishchev G, Ódor É, Ungar T, Lavernia E, Hahn H, Ivanisenko Y. Influence of carbon on the mechanical behavior and microstructure evolution of CoCrFeMnNi processed by high pressure torsion. *Materialia.* 2021;16:101059. <https://doi.org/10.1016/j.mtla.2021.101059>.
- [131] Kwon H, Asghari-Rad P, Park JM, Sathiyamoorthi P, Bae JW, Moon J, Zargaran A, Choi YT, Son S, Kim HS. Synergetic strengthening from grain refinement and nano-scale precipitates in non-equiatomic CoCrFeNiMo medium-entropy alloy. *Intermetallics.* 2021;135:107212. <https://doi.org/10.1016/j.intermet.2021.107212>.
- [132] Chandan AK, Hung PT, Kishore K, Kawasaki M, Chakraborty J, Gubicza J. On prominent TRIP effect and non-basal slip in a TWIP high entropy alloy during high-pressure torsion processing. *Mater Charact.* 2021;178:111284. <https://doi.org/10.1016/j.matchar.2021.111284>.
- [133] Picak S, Yilmaz HC, Karaman I. Simultaneous deformation twinning and martensitic transformation in CoCrFeMnNi high entropy alloy at high temperatures. *Scr Mater.* 2021;202:113995. <https://doi.org/10.1016/j.scriptamat.2021.113995>.
- [134] González-Masís J, Cubero-Sesin JM, Campos-Quirós A, Edalati K. Synthesis of biocompatible high-entropy alloy TiNbZrTaHf by high-pressure torsion. *Mater Sci Eng A.* 2021;825:141869. <https://doi.org/10.1016/j.msea.2021.141869>.
- [135] Maity T, Prashanth KG, Balci Ö, Cieślak G, Spychalski M, Kulik T, Eckert J. High-entropy eutectic composites with high strength and low Young's modulus. *MDPC.* 2021;3:e211. <https://doi.org/10.1002/mdp2.211>.
- [136] Edalati P, Mohammadi A, Tang Y, Floriano R, Fuji M, Edalati K. Phase transformation and microstructure evolution in ultrahard carbon-doped AlTiFeCoNi high-entropy alloy by high-pressure torsion. *Mater Lett.* 2021;302:130368. <https://doi.org/10.1016/j.matlet.2021.130368>.
- [137] Edalati P, Mohammadi A, Ketabchi M, Edalati K. Ultrahigh hardness in nanostructured dual-phase high-entropy alloy AlCrFeCoNiNb developed by high-pressure torsion. *J Alloys Compd.* 2021;884:161101. <https://doi.org/10.1016/j.jallcom.2021.161101>.

- [138] Asghari-Rad P, Sathiyamoorthi P, Nguyen NTC, Zargarán A, Kim TS, Kim HS. A powder-metallurgy-based fabrication route towards achieving high tensile strength with ultra-high ductility in high-entropy alloy. *Scr Mater.* 2021;190:69–74. <https://doi.org/10.1016/j.scriptamat.2020.08.038>.
- [139] Sathiyamoorthi P, Asghari-Rad P, Karthik GM, Zargarán A, Kim HS. Unusual strain-induced martensite and absence of conventional grain refinement in twinning induced plasticity high-entropy alloy processed by high-pressure torsion. *Mater Sci Eng A.* 2021;803:140570. <https://doi.org/10.1016/j.msea.2020.140570>.
- [140] Keil T, Bruder E, Laurent-Brocq M, Durst K. From diluted solid solutions to high entropy alloys: Saturation grain size and mechanical properties after high pressure torsion. *Scr Mater.* 2021;192:43–48. <https://doi.org/10.1016/j.scriptamat.2020.09.046>.
- [141] Zhao W, Han JK, Kuzminova YO, Evlashin SA, Zhilyaev AP, Pesin AM, Jang J, Liss KD, Kawasaki M. Significance of grain refinement on micro-mechanical properties and structures of additively-manufactured CoCrFeNi high-entropy alloy. *Mater Sci Eng A.* 2021;807:140898. <https://doi.org/10.1016/j.msea.2021.140898>.
- [142] Karthik GM, Asghari-Rad P, Sathiyamoorthi P, Zargarán A, Kim ES, Kim TS, Kim HS. Architected multi-metal CoCrFeMnNi-Inconel 718 lamellar composite by high-pressure torsion. *Scr Mater.* 2021;195:113722. <https://doi.org/10.1016/j.scriptamat.2021.113722>.
- [143] Taheriniya S, Davani FA, Hilke S, Hepp M, Gadelmeier C, Chellali MR, Boll T, Rösner H, Peterlechner M, Gammer C, Divinski SV, Butz B, Glatzel U, Hahn H, Wilde G. High entropy alloy nanocomposites produced by high pressure torsion. *Acta Mater.* 2021;208:116714. <https://doi.org/10.1016/j.actamat.2021.116714>.
- [144] Liu X, Ding H, Huang Y, Bai X, Zhang Q, Zhang H, Langdon TG, Cui J. Evidence for a phase transition in an AlCrFe₂Ni₂ high entropy alloy processed by high-pressure torsion. *J Alloys Compd.* 2021;867:159063. <https://doi.org/10.1016/j.jallcom.2021.159063>.
- [145] Rusakova HV, Fomenko LS, Smirnov SN, Podolskiy AV, Shapovalov YO, Tabachnikova ED, Tikhonovsky MA, Levenets AV, Zehetbauer MJ, Schafler E. Low temperature micromechanical properties of nanocrystalline CoCrFeNiMn high entropy alloy. *Mater Sci Eng A.* 2021;828:142116. <https://doi.org/10.1016/j.msea.2021.142116>.
- [146] Hung PT, Kawasaki M, Han JK, Lábár JL, Gubicza J. Microstructure evolution in a nanocrystalline CoCrFeNi multi-principal element alloy during annealing. *Mater Charact.* 2021;171:110807. <https://doi.org/10.1016/j.matchar.2020.110807>.
- [147] Asghari-Rad P, Nguyen NTC, Kim Y, Zargarán A, Sathiyamoorthi P, Kim HS. TiC-reinforced CoCrFeMnNi composite processed by cold-consolidation and subsequent annealing. *Mater Lett.* 2021;303:130503. <https://doi.org/10.1016/j.matlet.2021.130503>.
- [148] Li SC, Wang QL, Yao Y, Sang DD, Zhang HW, Zhang GZ, Wang C, Liu CL. Application of high-pressure technology in exploring mechanical properties of high-entropy alloys. *Tungsten.* 2022;in press. <https://doi.org/10.1007/s42864-021-00132-3>.
- [149] Nguyen NTC, Asghari-Rad P, Park H, Kim HS. Differential superplasticity in a multi-phase multi-principal element alloy by initial annealing. *J Mater Sci.* 2022;57:18154–18167. <https://doi.org/10.1007/s10853-022-07616-8>.

- [150] Shimizu H, Yuasa M, Miyamoto H, Edalati K. Corrosion behavior of ultrafine-grained CoCrFeMnNi high-entropy alloys fabricated by high-pressure torsion. *Materials*. 2022;15:1007. <https://doi.org/10.3390/ma15031007>.
- [151] Zhang Y, Liu M, Sun J, Li G, Zheng R, Xiao W, Ma C. Excellent thermal stability and mechanical properties of bulk nanostructured FeCoNiCu high entropy alloy. *Mater Sci Eng A*. 2022;835:142670. <https://doi.org/10.1016/j.msea.2022.142670>.
- [152] Chandan AK, Kishore K, Hung PT, Ghosh M, Chowdhury SG, Kawasaki M, Gubicza J. Effect of nickel addition on enhancing nano-structuring and suppressing TRIP effect in Fe₄₀Mn₄₀Co₁₀Cr₁₀ high entropy alloy during high-pressure torsion. *Int J Plast*. 2022;150:103193. <https://doi.org/10.1016/j.ijplas.2021.103193>.
- [153] Gao Z, Zhao Y, Park JM, Jeon AH, Murakami K, Komazaki S, Tsuchiya K, Ramamurty U, Jang J. Decoupling the roles of constituent phases in the strengthening of hydrogenated nanocrystalline dual-phase high-entropy alloys. *Scr Mater*. 2022;210:114472. <https://doi.org/10.1016/j.scriptamat.2021.114472>.
- [154] Akrami S, Edalati P, Shundo Y, Watanabe M, Ishihara T, Fuji M, Edalati K. Significant CO₂ photoreduction on a high-entropy oxynitride. *Chem Eng J*. 2022;449:137800. <https://doi.org/10.1016/j.cej.2022.137800>.
- [155] Akrami S, Murakami Y, Watanabe M, Ishihara T, Arita M, Fuji M, Edalati K. Defective high-entropy oxide photocatalyst with high activity for CO₂ conversion. *Appl Catal B*. 2022;303:120896. <https://doi.org/10.1016/j.apcatb.2021.120896>.
- [156] Keil T, Taheriniya S, Bruder E, Wilde G, Durst K. Effects of solutes on thermal stability, microstructure and mechanical properties in CrMnFeCoNi based alloys after high pressure torsion. *Acta Mater*. 2022;227:117689. <https://doi.org/10.1016/j.actamat.2022.117689>.
- [157] Son S, Asghari-Rad P, Zargaran A, Chen W, Kim HS. Superlative room temperature and cryogenic tensile properties of nanostructured CoCrFeNi medium-entropy alloy fabricated by powder high-pressure torsion. *Scr Mater*. 2022;213:114631. <https://doi.org/10.1016/j.scriptamat.2022.114631>.
- [158] Liang NN, Xu RR, Wu GZ, Gao XZ, Zhao YH. High thermal stability of nanocrystalline FeNi₂CoMo_{0.2}V_{0.5} high-entropy alloy by twin boundary and sluggish diffusion. *Mater Sci Eng A*. 2022;848:143399. <https://doi.org/10.1016/j.msea.2022.143399>.
- [159] Nguyen NTC, Asghari-Rad P, Zargaran A, Kim ES, Sathiyamoorthi P, Kim HS. Relation of phase fraction to superplastic behavior of multi-principal element alloy with a multi-phase structure. *Scr Mater*. 2022;221:114949. <https://doi.org/10.1016/j.scriptamat.2022.114949>.
- [160] Edalati P, Itagoe Y, Ishihara H, Ishihara T, Emami H, Arita M, Fuji M, Edalati K. Visible-light photocatalytic oxygen production on a high-entropy oxide with multiple-heterojunction introduction. *J Photochem Photobio A*. 2022;433:114167. <https://doi.org/10.1016/j.jphotochem.2022.114167>.
- [161] Hung PT, Kawasaki M, Han JK, Szabó Á, Lábár JL, Hegedűs Z, Gubicza J. Thermal stability of nanocrystalline CoCrFeNi multi-principal element alloy: effect of the degree of severe plastic deformation. *Intermetallics*. 2022;142:107445. <https://doi.org/10.1016/j.intermet.2021.107445>.

- [162] Straumal BB, Kulagin R, Baretzky B, Anisimova NY, Kiselevskiy MV, Klinger L, Straumal PB, Kogtenkova OA, Valiev RZ. Severe plastic deformation and phase transformations in high entropy alloys: a review. *Crystals*. 2022;12:54. <https://doi.org/10.3390/cryst12010054>.
- [163] Edalati P, Mohammadi A, Ketabchi M, Edalati K. Microstructure and microhardness of dual-phase high-entropy alloy by high-pressure torsion: twins and stacking faults in FCC and dislocations in BCC. *J Alloys Compd*. 2022;894:162413. <https://doi.org/10.1016/j.jallcom.2021.162413>.
- [164] Duan C, Reiberg M, Kutlesa P, Li X, Pippan R, Werner E. Strain-hardening properties of the high-entropy alloy MoNbTaTiVZr processed by high-pressure torsion. *Contin Mech Thermodyn*. 2022;34:475–489. <https://doi.org/10.1007/s00161-021-01065-5>.
- [165] Mohammadi A, Novelli M, Arita M, Bae JW, Kim HS, Grosdidier T, Edalati K. Gradient-structured high-entropy alloy with improved combination of strength and hydrogen embrittlement resistance. *Corros Sci*. 2022;200:110253. <https://doi.org/10.1016/j.corsci.2022.110253>.
- [166] Alijani F, Reihanian M, Gheisari K, Edalati K, Miyamoto H. Effect of homogenization on microstructure and hardness of arc-melted FeCoNiMn high entropy alloy during high-pressure torsion (HPT). *J Mater Eng Perform*. 2022;31:5080–5089. <https://doi.org/10.1007/s11665-021-06573-8>.
- [167] Mohammadi A, Edalati P, Arita M, Bae JW, Kim HS, Edalati K. Microstructure and defect effects on strength and hydrogen embrittlement of high-entropy alloy CrMnFeCoNi processed by high-pressure torsion. *Mater Sci Eng A*. 2022;844:143179. <https://doi.org/10.1016/j.msea.2022.143179>.
- [168] Levenets AV, Rusakova HV, Fomenko LS, Huang Y, Kolodiy V, Vasilenko RL, Tabachnikova ED, Tikhonovsky MA, Langdon TG. Structure and low-temperature micromechanical properties of as-cast and SPD-processed high-entropy $\text{Co}_{25-x}\text{Cr}_{25}\text{Fe}_{25}\text{Ni}_{25}\text{C}_x$ alloys. *Low Temp Phys*. 2022;48:560. <https://doi.org/10.1063/10.0011605>.
- [169] Bian YL, Feng ZD, Zhang NB, Li YX, Wang XF, Zhang BB, Cai Y, Lu L, Chen S, Yao XH, Luo SN. Ultrafast severe plastic deformation in high-entropy alloy $\text{Al}_{0.1}\text{CoCrFeNi}$ via dynamic equal channel angular pressing. *Mater Sci Eng A*. 2022;847:143221. <https://doi.org/10.1016/j.msea.2022.143221>.
- [170] Tian F, Varga LK, Chen N, Shen J, Vitos L. Empirical design of single phase high-entropy alloys with high hardness. *Intermetallics*. 2015;58:1–6. <https://doi.org/10.1016/j.intermet.2014.10.010>.
- [171] Yao HW, Qiao JW, Hawk JA, Zhou HF, Chen MW, Gao MC. Mechanical properties of refractory high-entropy alloys: experiments and modeling. *J Alloys Compd*. 2017;696:1139–1150. <https://doi.org/10.1016/j.jallcom.2016.11.188>.
- [172] Li Z, Zhao S, Ritchie RO, Meyers MA. Mechanical properties of high-entropy alloys with emphasis on face-centered cubic alloys. *Prog Mater Sci*. 2019;102:296–345. <https://doi.org/10.1016/j.pmatsci.2018.12.003>.
- [173] George EP, Curtin WA, Tasan CC. High entropy alloys: a focused review of mechanical properties and deformation mechanisms. *Acta Mater*. 2020;188:435–474. <https://doi.org/10.1016/j.actamat.2019.12.015>.

- [174] Zhilyaev AP, Langdon TG. Using high-pressure torsion for metal processing: fundamentals and applications. *Prog Mater Sci.* 2008;53:893–979. <https://doi.org/10.1016/j.pmatsci.2008.03.002>.
- [175] Edalati K, Z Horita. Scaling-up of high pressure torsion using ring shape. *Mater Trans.* 2009;50:92–95. <https://doi.org/10.2320/matertrans.MD200822>.
- [176] Edalati K, Horita Z, Mine Y. High-pressure torsion of hafnium. *Mater Sci Eng A.* 2010;527:2136–2141. <https://doi.org/10.1016/j.msea.2009.11.060>.
- [177] Lee S, Edalati K, Horita Z. Microstructures and mechanical properties of pure V and Mo processed by high-pressure torsion. *Mater Trans.* 2010;51:1072–1079. <https://doi.org/10.2320/matertrans.M2009375>.
- [178] Chen L, Ping L, Ye T, Lingfeng L, Kemin X, Meng Z. Observations on the ductility and thermostability of tungsten processed from micropowder by improved high-pressure torsion. *Rare Met Mater Eng.* 2016;45:3089–3094. [https://doi.org/10.1016/S1875-5372\(17\)30059-0](https://doi.org/10.1016/S1875-5372(17)30059-0).
- [179] Edalati K, Yokoyama Y, Horita Z. High-pressure torsion of machining chips and bulk discs of amorphous $Zr_{50}Cu_{30}Al_{10}Ni_{10}$. *Mater Trans.* 2010;51:23–26. <https://doi.org/10.2320/matertrans.MB200914>.
- [180] Wang YB, Qu DD, Wang XH, Cao Y, Liao XZ, Kawasaki M, Ringer SP, Shan ZW, Langdon TG, Shen J. Introducing a strain-hardening capability to improve the ductility of bulk metallic glasses via severe plastic deformation. *Acta Mater.* 2012;60:253–260. <https://doi.org/10.1016/j.actamat.2011.09.026>.
- [181] Edalati K, Horita Z. Correlations between hardness and atomic bond parameters of pure metals and semi-metals after processing by high-pressure torsion. *Scr Mater.* 2011;64:161–164. <https://doi.org/10.1016/j.scriptamat.2010.09.034>.
- [182] Ikoma Y, Hayano K, Edalati K, Saito K, Guo Q, Horita Z. Phase transformation and nanograin refinement of silicon by processing through high-pressure torsion. *Appl Phys Lett.* 2012;101:121908. <https://doi.org/10.1063/1.4754574>.
- [183] Blank VD, Churkin VD, BA Kulnitskiy, Perezhogin IA, Kirichenko AN, Erohin SV, Sorokin PB, Popov MY. Pressure-induced transformation of graphite and diamond to onions. *Crystals.* 2018;8:68. <https://doi.org/10.3390/cryst8020068>.
- [184] Gao Y, Ma Y, An Q, Levitas VI, Zhang Y, Feng B, Chaudhuri J, Goddard WA. III. Shear driven formation of nano-diamonds at sub-gigapascals and 300 K. *Carbon.* 2019;146:364–368. <https://doi.org/10.1016/j.carbon.2019.02.012>.
- [185] Dwivedi SK, Vishwakarma M. Hydrogen embrittlement in different materials: a review. *Int J Hydrogen Energy.* 2108;43: 21603–21616. <https://doi.org/10.1016/j.ijhydene.2018.09.201>.
- [186] Martin ML, Dadfarnia M, Nagao A, Wang S, Sofronis P. Enumeration of the hydrogen-enhanced localized plasticity mechanism for hydrogen embrittlement in structural materials. *Acta Mater.* 2019;165:734–750. <https://doi.org/10.1016/j.actamat.2018.12.014>.
- [187] Djukic MB, Bakic GM, Zeravcic VS, Sedmak A, Rajicic B. The synergistic action and interplay of hydrogen embrittlement mechanisms in steels and iron: localized plasticity and decohesion. *Eng Fract Mech.* 2019;A216:106528. <https://doi.org/10.1016/j.engfracmech.2019.106528>.
- [188] Zhao Y, Lee DH, Seok MY, Lee J, Phaniraj MP, Suh JY, Ha HY, Kim JY, Ramamurty U, Jang J. Resistance of CoCrFeMnNi high-entropy alloy to gaseous hydrogen embrittlement. *Scr Mater.* 2017;135:54–58. <https://doi.org/10.1016/j.scriptamat.2017.03.029>.

- [189] Luo H, Lu WJ, Fang XF, Ponge D, Li ZM, Raabe D. Beating hydrogen with its own weapon: nano-twin gradients enhance embrittlement resistance of a high-entropy alloy. *Mater Today*. 2018;21:1003–1009. <https://doi.org/10.1016/j.mattod.2018.07.015>.
- [190] Mine Y, Haraguchi D, Ideguchi T, Horita N, Horita Z, Takashima K. Hydrogen embrittlement of ultrafine-grained austenitic stainless steels processed by high-pressure torsion at moderate temperature. *ISIJ Int*. 2016;56:1083–1090. <https://doi.org/10.2355/isijinternational.ISIJINT-2015-664>
- [191] Bai Y, Momotani Y, Chen MC, Shibata A, Tsuji N. Effect of grain refinement on hydrogen embrittlement behaviors of high-Mn TWIP steel. *Mater Sci Eng A*. 2016;651:935–944. <https://doi.org/10.1016/j.msea.2015.11.017>.
- [192] Valiev RZ. Nanostructuring of metals by severe plastic deformation for advanced properties. *Nat Mater*. 2004;3:511–516. <https://doi.org/10.1038/nmat1180>.
- [193] Meyers MA, Mishra A, Benson DJ. The deformation physics of nanocrystalline metals: experiments, analysis, and computations. *JOM*. 2006;58(4):41–48. <https://doi.org/10.1007/s11837-006-0214-6>.
- [194] Ma E. Eight routes to improve the tensile ductility of bulk nanostructured metals and alloys. *JOM*. 2006;58(4):49–53. <https://doi.org/10.1007/s11837-006-0215-5>.
- [195] Valiev RZ, Murashkin MY, Kilmametov A, Straumal B, Chinh NQ, Langdon TG. Unusual super-ductility at room temperature in an ultrafine-grained aluminum alloy. *J Mater Sci*. 2010;45:4718–4724. <https://doi.org/10.1007/s10853-010-4588-z>.
- [196] Bryła K, Morgiel J, Faryna M, Edalati K, Horita Z. Effect of high-pressure torsion on grain refinement, strength enhancement and uniform ductility of EZ magnesium alloy. *Mater Lett*. 2018;212:323–326. <https://doi.org/10.1016/j.matlet.2017.10.113>.
- [197] Valiev R, Semenova IP, Jakushina E, Latysh VV, Rack HJ, Lowe TC, Petruželka J, Dluhoš L, Hrušák D, Sochová J. Nanostructured SPD processed titanium for medical implants. *Mater Sci Forum*. 2008;584-586:49–54. <https://doi.org/10.4028/www.scientific.net/MSF.584-586.49>.
- [198] Estrin Y, Kim HE, Lapovok R, Ng HP, Jo JH. Mechanical strength and biocompatibility of ultrafine-grained commercial purity titanium. *BioMed Res Int*. 2013;2013:914764. <https://doi.org/10.1155/2013/914764>.
- [199] Kubacka D, Yamamoto A, Wieceński P, Garbacz H. Biological behavior of titanium processed by severe plastic deformation. *Appl Surf Sci*. 2019;472:54–63. <https://doi.org/10.1016/j.apsusc.2018.04.120>.
- [200] Lowe TC, Valiev RZ, Li X, Ewing BR. Commercialization of bulk nanostructured metals and alloys. *MRS Bull*. 2021;46:265–272. <https://doi.org/10.1557/s43577-021-00060-0>.
- [201] Long M, Rack HJ. Titanium alloys in total joint replacement - a materials science perspective. *Biomaterials*. 1998;19:1621–1639. [https://doi.org/10.1016/S0142-9612\(97\)00146-4](https://doi.org/10.1016/S0142-9612(97)00146-4).
- [202] Todai M, Nagase T, Hori T, Matsugaki A, Sekita A, Nakano T. Novel TiNbTaZrMo high-entropy alloys for metallic biomaterials. *Scr Mater*. 2017;129:65–68. <https://doi.org/10.1016/j.scriptamat.2016.10.028>.
- [203] Newell R, Wang Z, Arias I, Mehta A, Sohn Y, Florczyk S. Direct-contact cytotoxicity evaluation of CoCrFeNi-based multi-principal element alloys. *J Funct Biomater*. 2018;9:59. <https://doi.org/10.3390/jfb9040059>.

- [204] Hori T, Nagase T, Todai M, Matsugaki A, Nakano T. Development of non-equiatomic Ti-Nb-Ta-Zr-Mo high-entropy alloys for metallic biomaterials. *Scr Mater.* 2019;172:83–87. <https://doi.org/10.1016/j.scriptamat.2019.07.011>.
- [205] Nagase T, Iijima Y, Matsugaki A, Ameyama K, Nakano T. Design and fabrication of Ti-Zr-Hf-Cr-Mo and Ti-Zr-Hf-Co-Cr-Mo high-entropy alloys as metallic biomaterials. *Mater Sci Eng C.* 2020;107:110322. <https://doi.org/10.1016/j.msec.2019.110322>.
- [206] Alagarsamy K, Fortier A, Komarasamy M, Kumar N, Mohammad A, Banerjee S, Han HC, Mishra RS. Mechanical properties of high entropy alloy $\text{Al}_{0.1}\text{CoCrFeNi}$ for peripheral vascular stent application. *Cardiovasc Eng Technol.* 2016;7:448–454. <https://doi.org/10.1007/s13239-016-0286-6>.
- [207] Wang SP, Xu J. TiZrNbTaMo high-entropy alloy designed for orthopedic implants: as-cast microstructure and mechanical properties. *Mater Sci Eng C.* 2017;73:80–89. <https://doi.org/10.1016/j.msec.2016.12.057>.
- [208] Nagase T, Todai M, Hori T, Nakano T. Microstructure of equiatomic and non-equiatomic Ti-Nb-Ta-Zr-Mo high-entropy alloys for metallic biomaterials. *J Alloys Compd.* 2018;753:412–421. <https://doi.org/10.1016/j.jallcom.2018.04.082>.
- [209] Yuan Y, Wu Y, Yang Z, Liang X, Lei Z, Huang H, Wang H, Liu X, An K, Wu W, Lu Z. Formation, structure and properties of biocompatible TiZrHfNbTa high-entropy alloys. *Mater Res Lett.* 2019;7:225–231. <https://doi.org/10.1080/21663831.2019.1584592>.
- [210] Motallebzadeh A, Peighambaroust NS, Sheikh S, Murakami H, Guo S, Canadinc D. Microstructural, mechanical and electrochemical characterization of TiZrTaHfNb and $\text{Ti}_{1.5}\text{ZrTa}_{0.5}\text{Hf}_{0.5}\text{Nb}_{0.5}$ refractory high-entropy alloys for biomedical applications. *Intermetallics.* 2019;113:106572. <https://doi.org/10.1016/j.intermet.2019.106572>.
- [211] Edalati K, Uehiro R, Fujiwara K, Ikeda Y, Li HW, Sauvage X, Valiev RZ, Akiba E, Tanaka I, Horita Z. Ultra-severe plastic deformation: evolution of microstructure, phase transformation and hardness in immiscible magnesium-based systems. *Mater Sci Eng A.* 2017;701:158–166. <https://doi.org/10.1016/j.msea.2017.06.076>.
- [212] Edalati K, Emami H, Staykov A, Smith DJ, Akiba E, Horita Z. Formation of metastable phases in magnesium-titanium system by high-pressure torsion and their hydrogen storage performance. *Acta Mater.* 2015;50:150–156. <https://doi.org/10.1016/j.actamat.2015.07.060>.
- [213] Edalati K, Emami H, Ikeda Y, Iwaoka H, Tanaka I, Akiba E, Horita Z. New nanostructured phases with reversible hydrogen storage capability in immiscible magnesium-zirconium system produced by high-pressure torsion. *Acta Mater.* 2016;108:293–303. <https://doi.org/10.1016/j.actamat.2016.02.026>.
- [214] Kormout KS, Pippan R, Bachmaier A. Deformation-induced supersaturation in immiscible material systems during high-pressure torsion. *Adv Eng Mater.* 2017;19:1600675. <https://doi.org/10.1002/adem.201600675>.
- [215] Oberdorfer B, Lorenzoni B, Unger K, Sprengel W, Zehetbauer M, Pippan R, Wurschum R. Absolute concentration of free volume-type defects in ultrafine-grained Fe prepared by high-pressure torsion. *Scr Mater.* 2010;63:452–455. <https://doi.org/10.1016/j.scriptamat.2010.05.007>.
- [216] Divinski SV, Reglitz G, Rösner H, Estrin Y, Wilde G. Ultra-fast diffusion channels in pure Ni severely deformed by equal-channel angular pressing. *Acta Mater.* 2011;59:1974–1985. <https://doi.org/10.1016/j.actamat.2010.11.063>.

- [217] Straumal BB, Mazilkin AA, Baretzky B, Schütz G, Rabkin E, Valiev RZ. Accelerated diffusion and phase transformations in Co-Cu alloys driven by the severe plastic deformation. *Mater Trans*. 2012;53:63–71. <https://doi.org/10.2320/matertrans.MD201111>.
- [218] Figueiredo RB, Pereira PHR, Aguilar MTP, Cetlin PR, Langdon TG. Using finite element modeling to examine the temperature distribution in quasi-constrained high-pressure torsion. *Acta Mater*. 2012;60:3190–3198. <https://doi.org/10.1016/j.actamat.2012.02.027>.
- [219] Edalati K, Hashiguchi Y, Pereira PHR, Horita Z, Langdon TG. Effect of temperature rise on microstructural evolution during high-pressure torsion. *Mater Sci Eng A*. 2018;714:167–171. <https://doi.org/10.1016/j.msea.2017.12.095>.
- [220] Saini M, Singh Y, Arora P, Arora V, Jain K. Implant biomaterials: a comprehensive review. *World J Clin Cases*. 2015: 52–57. <https://doi.org/10.12998/wjcc.v3.i1.52>.
- [221] Schlapbach L, Züttel A. Hydrogen-storage materials for mobile applications. *Nature*. 2001;414:353–358. <https://doi.org/10.1038/35104634>.
- [222] von Colbe JB, Ares JR, Barale J, Baricco M, Buckley C, Capurso G, Gallandat N, Grant DM, Guzik MN, Jacob I, Jensen EH, Jensen T, Jepsen J, Klassen T, Lototskyy MV, Manickam K, Montone A, Puszkiel J, Sartori S, Sheppard DA, Stuart A, Walker G, Webb CJ, Yang H, Yartys V, Züttel A, Dornheim M. Application of hydrides in hydrogen storage and compression: achievements, outlook and perspectives. *Int J Hydrog Energy*. 2019;44: 7780–7808. <https://doi.org/10.1016/j.ijhydene.2019.01.104>.
- [223] Hirscher M, Yartys VA, Baricco M, von Colbe JB, Blanchard D, Bowman Jr. RC, Broom DP, Buckley CE, Chang F, Chen P, Cho YW, Crivello JC, Cuevas F, David WIF, de Jongh PE, Denys RV, Dornheim M, Felderhoff M, Filinchuk Y, Froudakis GE, Grant DM, Gray EMA, Hauback BC, He T, Humphries TD, Jensen TR, Kim S, Kojima Y, Latroche M, Li HW, Lototskyy MV, Makepeace JW, Møller KT, Naheed L, Ngene P, Noréus D, Nygård MM, Orimo S, Paskevicius M, Pasquini L, Ravnsbæk DB, Sofianos MV, Udovic TJ, Vegge T, Walker GS, Webb CJ, Weidenthaler C, Zlotea C. Materials for hydrogen-based energy storage - past, recent progress and future outlook. *J Alloys Compd*. 2020;827:153548. <https://doi.org/10.1016/j.jallcom.2019.153548>.
- [224] Jain IP, Lal C, Jain A. Hydrogen storage in Mg: a most promising material. *Int J Hydrogen Energy*. 2010;35:5133–5144. <https://doi.org/10.1016/j.ijhydene.2009.08.088>.
- [225] Pasquini L, Sakaki K, Akiba E, Allendorf MD, Alvares E, Ares JR, Babai D, Baricco M, von Colbe JB, Bereznitsky M, Buckley CE, Cho YW, Cuevas F, de Rango P, Dematteis EM, Denys RV, Dornheim M, Fernández JF, Hariyadi A, Hauback BC, Heo TW, Hirscher M, Humphries TD, Huot J, Jacob I, Jensen TR, Jerabek P, Kang SY, Keilbart N, Kim H, Latroche M, Leardini F, Li H, Ling S, Lototskyy MV, Mullen R, Orimo S, Paskevicius M, Pistidda C, Polanski M, Puszkiel J, Rabkin E, Sahlberg M, Sartori S, Santhosh A, Sato T, Shneck RZ, Sørby MH, Shang Y, Stavila V, Suh JY, Suwarno S, Thu LT, Wan LF, Webb CJ, Witman M, Wan CB, Wood BC, Yartys VA. Magnesium- and intermetallic alloys-based hydrides for energy storage: modelling, synthesis and properties. *Prog Energy*. 2022;4: 032007. <https://doi.org/10.1088/2516-1083/ac7190>.
- [226] Skripnyuk VM, Rabkin E, Estrin Y, Lapovok R. The effect of ball milling and equal channel angular pressing on the hydrogen absorption/desorption properties of Mg-4.95 wt% Zn-0.71 wt% Zr (ZK60) alloy. *Acta Mater*. 2004;52:405–414. <https://doi.org/10.1016/j.actamat.2003.09.025>.

- [227] Grill A, Horky J, Panigrahi A, Krexner G, Zehetbauer M. Long-term hydrogen storage in Mg and ZK60 after severe plastic deformation. *Int J Hydrog Energy*. 2015;40:17144–17152. <https://doi.org/10.1016/j.ijhydene.2015.05.145>.
- [228] Skryabina N, Aptukov V, Romanov P, Fruchart D, de Rango P, Girard G, Grandini C, Sandim H, Huot J, Lang J, Cantelli R, Leardini F. Microstructure optimization of Mg-alloys by the ECAP process including numerical simulation, SPD treatments, characterization, and hydrogen sorption properties. *Molecules*. 2019;24:89. <https://doi.org/10.3390/molecules24010089>.
- [229] Leiva DR, Jorge AM, Ishikawa TT, Huot J, Fruchart D, Miraglia S, Kiminami CS, Botta WJ. Nanoscale grain refinement and H-sorption properties of MgH₂ processed by high-pressure torsion and other mechanical routes. *Adv Eng Mater*. 2010;12:786–792. <https://doi.org/10.1002/adem.201000030>.
- [230] Panda S, Fundenberger JJ, Zhao Y, Zou J, Toth LS, Grosdidier T. Effect of initial powder type on the hydrogen storage properties of high-pressure torsion consolidated Mg. *Int J Hydrog Energy*. 2017;42:22438–22448. <https://doi.org/10.1016/j.ijhydene.2017.05.097>.
- [231] Révész Á, Gajdics M. High-pressure torsion of non-equilibrium hydrogen storage materials: a review. *Energies*. 2012;14:819. <https://doi.org/10.3390/en14040819>.
- [232] Huot J, Cuevas F, Deledda S, Edalati K, Filinchuk Y, Grosdidier T, Hauback BC, Heere M, Jensen TR, Latroche M, Sartori S. Mechanochemistry of metal hydrides: recent advances. *Materials*. 2019;12:2778. <https://doi.org/10.3390/ma12172778>.
- [233] Edalati K, Uehiro R, Ikeda Y, Li HW, Emami H, Filinchuk Y, Arita M, Sauvage X, Tanaka I, Akiba E, Horita Z. Design and synthesis of a magnesium alloy for room temperature hydrogen storage. *Acta Mater*. 2018;149:88–96. <https://doi.org/10.1016/j.actamat.2018.02.033>.
- [234] Floriano R, Zepon G, Edalati K, Fontana GLBG, Mohammadi A, Ma Z, Li HW, Contieri R. Hydrogen storage in TiZrNbFeNi high entropy alloys, designed by thermodynamic calculations. *Int J Hydrogen Energy*. 2020;45:33759–33770. <https://doi.org/10.1016/j.ijhydene.2020.09.047>.
- [235] Floriano R, Zepon G, Edalati K, Fontana GLBG, Mohammadi A, Ma Z, Li HW, Contieri RJ. Hydrogen storage properties of new A₃B₂-type TiZrNbCrFe high-entropy alloy. *Int J Hydrogen Energy*. 2021;46:23757–23766. <https://doi.org/10.1016/j.ijhydene.2021.04.181>.
- [236] Mohammadi A, Ikeda Y, Edalati P, Mito M, Grabowski B, Li HW, Edalati K. High-entropy hydrides for fast and reversible hydrogen storage at room temperature: binding-energy engineering via first-principles calculations and experiments. *Acta Mater*. 2022;236:118117. <https://doi.org/10.1016/j.actamat.2022.118117>.
- [237] Edalati P, Mohammadi A, Li Y, Li HW, Floriano R, Fuji M, Edalati K. High-entropy alloys as anode materials of nickel - metal hydride batteries. *Scr Mater*. 2022;209:114387. <https://doi.org/10.1016/j.scriptamat.2021.114387>.
- [238] Goetzberger A, Hebling C, Schock HW. Photovoltaic materials, history, status and outlook. *Mater Sci Eng R*. 2003;40:1–46. [https://doi.org/10.1016/S0927-796X\(02\)00092-X](https://doi.org/10.1016/S0927-796X(02)00092-X).
- [239] Parida B, Iniyar S, Goic R. A review of solar photovoltaic technologies. *Renew Sust Energ Rev*. 2011;15:1625–1636. <https://doi.org/10.1016/j.rser.2010.11.032>.
- [240] Polman A, Knight M, Garnett EC, Ehrler B, Sinke WC. Photovoltaic materials: present efficiencies and future challenges. *Science*. 2016;352:aad4424. <https://doi.org/10.1126/science.aad4424>.

- [241] Wang Q, Watanabe M, Edalati K. Visible-light photocurrent in nanostructured high-pressure TiO₂-II (columbite) phase. *J Phys Chem C*. 2020;124:13930–13935. <https://doi.org/10.1021/acs.jpcc.0c03923>.
- [242] Fujita I, Edalati P, Wang Q, Watanabe M, Arita M, Munetoh S, Ishihara T, Edalati K. Novel black bismuth oxide (Bi₂O₃) with enhanced photocurrent generation, produced by high-pressure torsion straining. *Scr Mater*. 2020;187:366–370. <https://doi.org/10.1016/j.scriptamat.2020.06.052>.
- [243] Fujishima A, Rao TN, Tryk DA. Titanium dioxide photocatalysis. *J Photochem Photobiol C*. 2000;1:1–21. [https://doi.org/10.1016/S1389-5567\(00\)00002-2](https://doi.org/10.1016/S1389-5567(00)00002-2).
- [244] Kumar A, Choudhary P, Kumar A, Camargo PHC, Krishnan V. Recent advances in plasmonic photocatalysis based on TiO₂ and noble metal nanoparticles for energy conversion, environmental remediation, and organic synthesis. *Small*. 2022;18:2101638. <https://doi.org/10.1002/sml.202101638>.
- [245] Maeda K, Domen K. Photocatalytic water splitting: recent progress and future challenges. *J Phys Chem Lett*. 2010;1:2655–2661. <https://doi.org/10.1021/jz1007966>.
- [246] Wang D, Liu Z, Du S, Zhang Y, Li H, Xiao Z, Chen W, Chen R, Wang Y, Zou Y. Low-temperature synthesis of small-sized high-entropy oxides for water oxidation. *J Mater Chem A*. 2019;7:24211–24216. <https://doi.org/10.1039/C9TA08740K>.
- [247] Ding Z, Bian J, Shuang S, Liu X, Hu Y, Sun C, Yang Y. High entropy intermetallic–oxide core-shell nanostructure as superb oxygen evolution reaction catalyst. *Adv Sustain Syst*. 2020;4:1900105. <https://doi.org/10.1002/adsu.201900105>.
- [248] Fang G, Gao J, Lv J, Jia H, Li H, Liu W, Xie G, Chen Z, Huang Y, Yuan Q, Liu X, Lin X, Sun S, Qiu HJ. Multi-component nanoporous alloy/(oxy)hydroxide for bifunctional oxygen electrocatalysis and rechargeable Zn-air batteries. *Appl Catal B*. 2020;268:118431. <https://doi.org/10.1016/j.apcatb.2019.118431>.
- [249] Okejiri F, Zhang Z, Liu J, Liu M, Yang S, Dai S. Room-temperature synthesis of high-entropy perovskite oxide nanoparticle catalysts through ultrasonication-based method. *ChemSusChem*. 2020;13:111–115. <https://doi.org/10.1002/cssc.201902705>.
- [250] Xu H, Zhang Z, Liu J, Do-Thanh CL, Chen H, Xu S, Lin Q, Jiao Y, Wang J, Wang Y, Chen Y, Dai S. Entropy-stabilized single-atom Pd catalysts via high-entropy fluorite oxide supports. *Nat Commun*. 2020;11:3908. <https://doi.org/10.1038/s41467-020-17738-9>.
- [251] Chen H, Jie K, Jafta CJ, Yang Z, Yao S, Liu M, Zhang Z, Liu J, Chi M, Fu J, Dai S. An ultrastable heterostructured oxide catalyst based on high-entropy materials: a new strategy toward catalyst stabilization via synergistic interfacial interaction. *Appl Catal B*. 2020;276:119155. <https://doi.org/10.1016/j.apcatb.2020.119155>.
- [252] Zheng Y, Yi Y, Fan M, Liu H, Li X, Zhang R, Li M, Qiao ZA. A high-entropy metal oxide as chemical anchor of polysulfide for lithium-sulfur batteries. *Energy Storage Mater*. 2019;23:678–683. <https://doi.org/10.1016/j.ensm.2019.02.030>.
- [253] Chen H, Lin W, Zhang Z, Jie K, Mullins DR, Sang X, Yang SZ, Jafta CJ, Bridges CA, Hu X. Mechanochemical synthesis of high entropy oxide materials under ambient conditions: dispersion of catalysts via entropy maximization. *ACS Mater Lett* 2019;1:83–88. <https://doi.org/10.1021/acsmaterialslett.9b00064>.
- [254] Lal MS, Sundara R. High entropy oxides - a cost-effective catalyst for the growth of high yield carbon nanotubes and their energy applications. *ACS Appl Mater Interfaces*. 2019;11:30846–30857. <https://doi.org/10.1021/acsami.9b08794>.

- [255] Shu Y, Bao J, Yang S, Duan X, Zhang P. Entropy-stabilized metal-CeO_x solid solutions for catalytic combustion of volatile organic compounds. *AIChE J.* 2021;67:e17046. <https://doi.org/10.1002/aic.17046>.
- [256] Sun Y, Dai S. High-entropy materials for catalysis: A new frontier. *Sci Adv.* 2021;7:20.
- [257] Liu Z, Deng Z, Davis SJ, Giron C, Ciais P. Monitoring global carbon emissions in 2021. *Nat Rev Earth Environ.* 2022;3:217–219. <https://doi.org/10.1038/s43017-022-00285-w>.
- [258] Park JH, Yang J, Kim, Gim H, Choi WY, Lee JW. Review of recent technologies for transforming carbon dioxide to carbon materials. *Chem Eng J.* 2022;427:1300980. <https://doi.org/10.1016/j.cej.2021.130980>.
- [259] Li K, Peng B, Peng T. Recent advances in heterogeneous photocatalytic CO₂ conversion to solar fuels. *ACS Catal.* 2016;6:7485–7527. <https://doi.org/10.1021/acscatal.6b02089>.
- [260] Akrami S, Watanabe M, Ling TH, Ishihara T, Arita M, Fuji M, Edalati K. High pressure TiO₂-II polymorph as an active photocatalyst for CO₂ to CO conversion. *Appl Catal B.* 2021;298:120566. <https://doi.org/10.1016/j.apcatb.2021.120566>.
- [261] Akrami S, Murakami Y, Watanabe M, Ishihara T, Arita M, Guo Q, Fuji M, Edalati K. Enhanced CO₂ conversion on highly-strained and oxygen-deficient BiVO₄ photocatalyst. *Chem Eng J.* 2022;442:136209. <https://doi.org/10.1016/j.cej.2022.136209>.
- [262] Levitas VI. High-pressure mechanochemistry: conceptual multiscale theory and interpretation of experiments. *Phys. Rev. B.* 2004;70:184118. <https://doi.org/10.1103/PhysRevB.70.184118>.
- [263] Bahers TL, Rérat M, Sautet P. Semiconductors used in photovoltaic and photocatalytic devices: assessing fundamental properties from DFT. *J. Phys. Chem. C.* 2014;118:5997–6008. <https://doi.org/10.1021/jp409724c>.
- [264] Niu X, Bai X, Zhou Z, Wang J. Rational design and characterization of direct Z-scheme photocatalyst for overall water splitting from excited state dynamics simulations. *ACS Catal.* 2020;10:1976–1983. <https://doi.org/10.1021/acscatal.9b04753>.
- [265] Pavone M, Toroker MC. Toward ambitious multiscale modeling of nanocrystal catalysts for water splitting. *ACS Energy Lett.* 2020;5:2042–2044. <https://doi.org/10.1021/acsenenergylett.0c01086>.

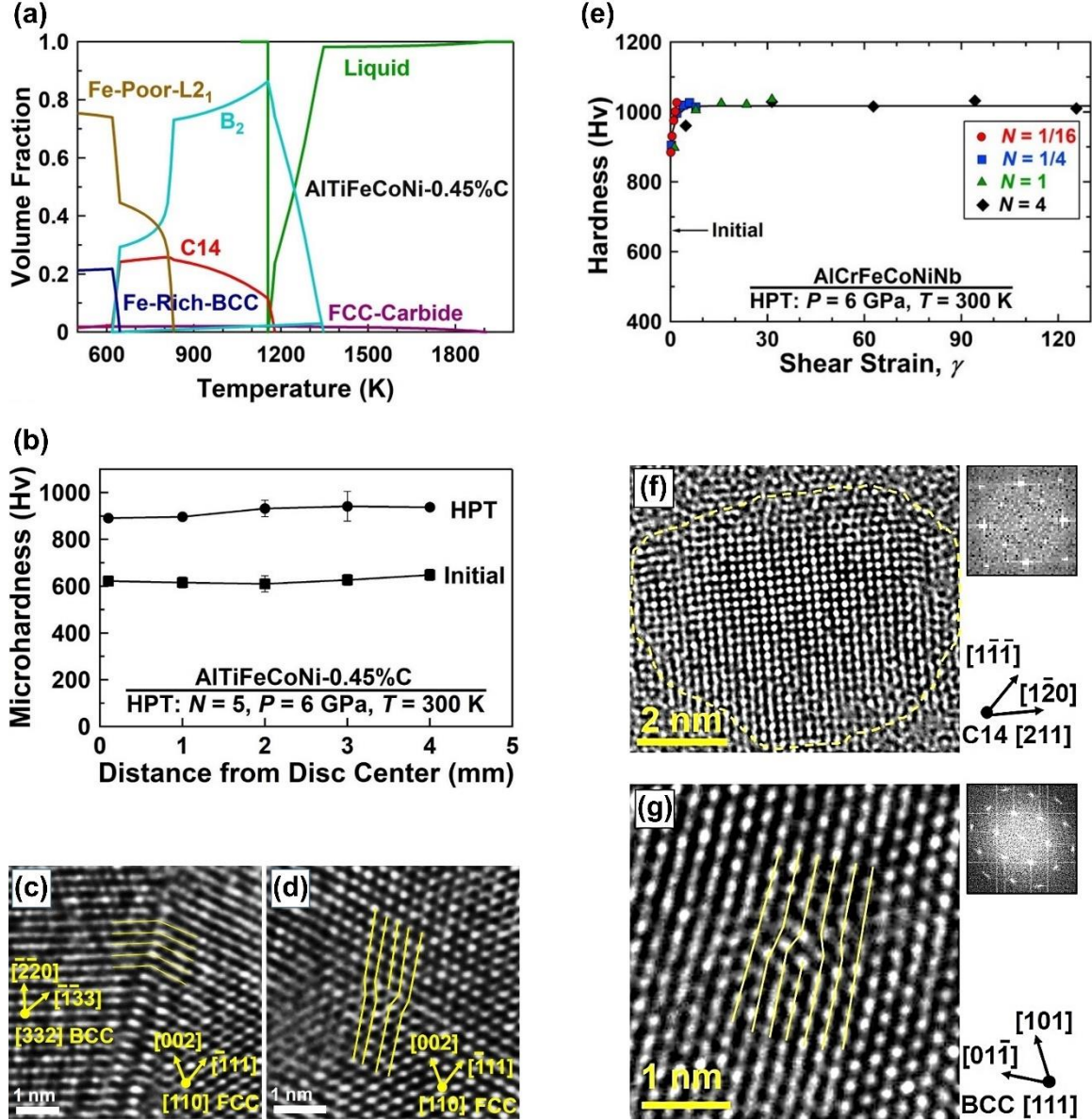


Fig. 1 Development of ultrahard high-entropy alloys by severe plastic deformation. **a** Phase diagram of AlTiFeCoNi doped with 0.45 wt% of carbon calculated by CALPHAD. Reproduced with permission from Ref. [136]. Copyright 2021, Elsevier. **b** Hardness of carbon-doped AlTiFeCoNi before and after HPT processing. Reproduced with permission from Ref. [136]. Copyright 2021, Elsevier. **c, d** High-resolution lattice images of HPT-processed carbon-doped AlTiFeCoNi showing the presence of interphases and dislocations. Reproduced with permission from Ref. [136]. Copyright 2021, Elsevier. **e** Hardness against shear strain for AlCrFeCoNiNb processed by HPT for various turns, N . Reproduced with permission from Ref. [137]. Copyright 2021, Elsevier. **f, g** Lattice images and corresponding diffractograms for AlCrFeCoNiNb processed by HPT for $N = 4$ showing the presence of nanograins and dislocations. Reproduced with permission from Ref. [137]. Copyright 2021, Elsevier.

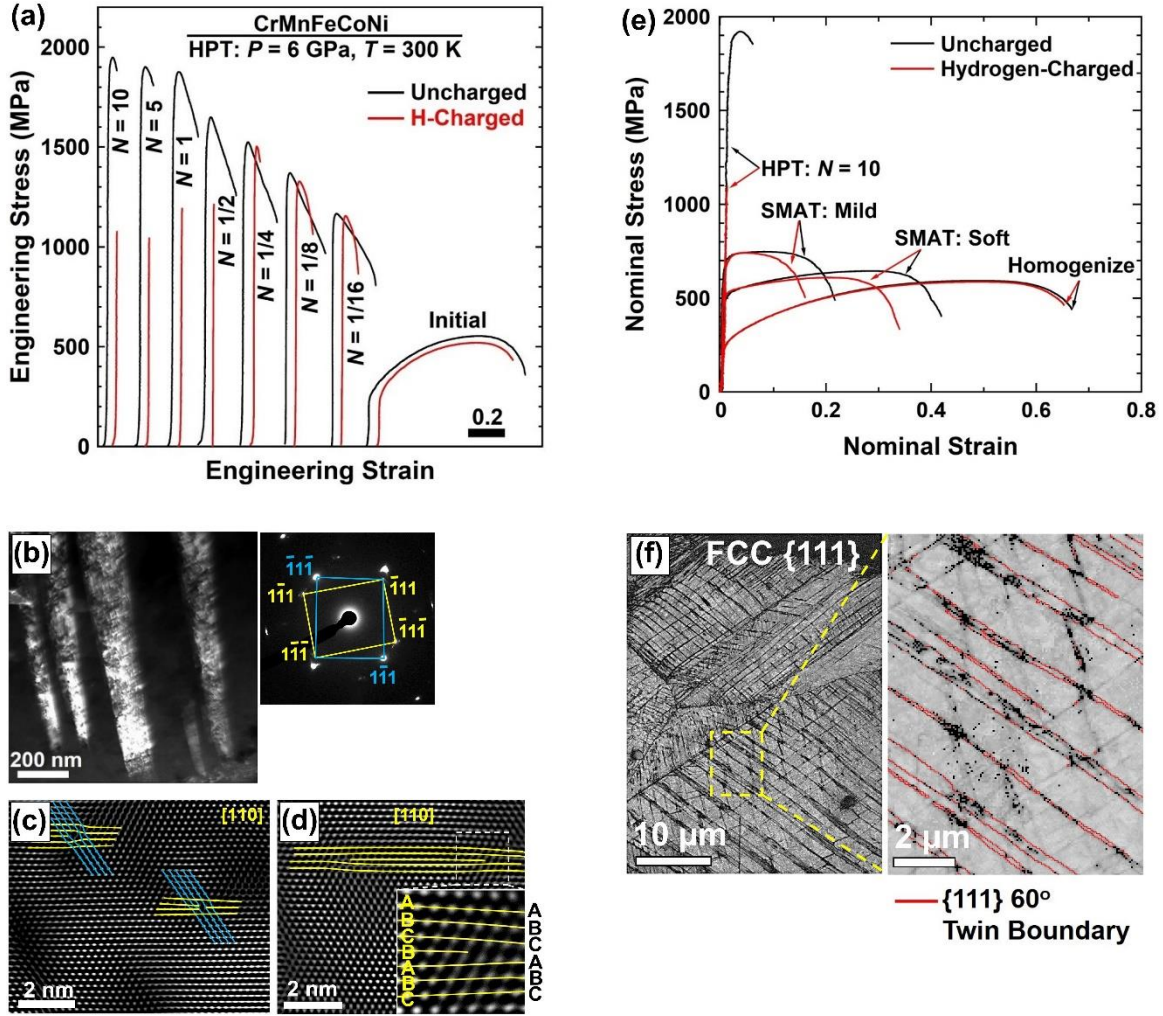


Fig. 2 Development of high yield strength and good resistance to hydrogen embrittlement in high-entropy alloys by severe plastic deformation. **a** Tensile stress-strain curves before and after hydrogen charging for Cantor alloy CrMnFeCoNi processed by HPT for various rotations, N . Reproduced with permission from Ref. [167]. Copyright 2022, Elsevier. **b** dark-field image and corresponding selected area electron diffraction patterns for CrMnFeCoNi processed with HPT for $N = 1/16$, showing the presence of twins. Reproduced with permission from Ref. [167]. Copyright 2022, Elsevier. **c, d** High-resolution lattice images of CrMnFeCoNi processed by HPT for $N = 1/4$, showing the presence of Lomer-Cottrell locks and D-Frank partial dislocations. Reproduced with permission from Ref. [167]. Copyright 2022, Elsevier. **e** Tensile stress-strain curves before and after hydrogen charging for CrMnFeCoNi processed by homogenization, soft SMAT (40 μ m ultrasonic amplitude for 30 s), mild SMAT (60 μ m ultrasonic amplitude for 60 s) and intense HPT ($N = 10$). Reproduced with permission from Ref. [165]. Copyright 2022, Elsevier. **f** Band contrast image and {111} twin boundary mapping by electron backscatter diffraction in scanning electron microscopy for CrMnFeCoNi processed by SMAT under mild conditions. Reproduced with permission from Ref. [165]. Copyright 2022, Elsevier.

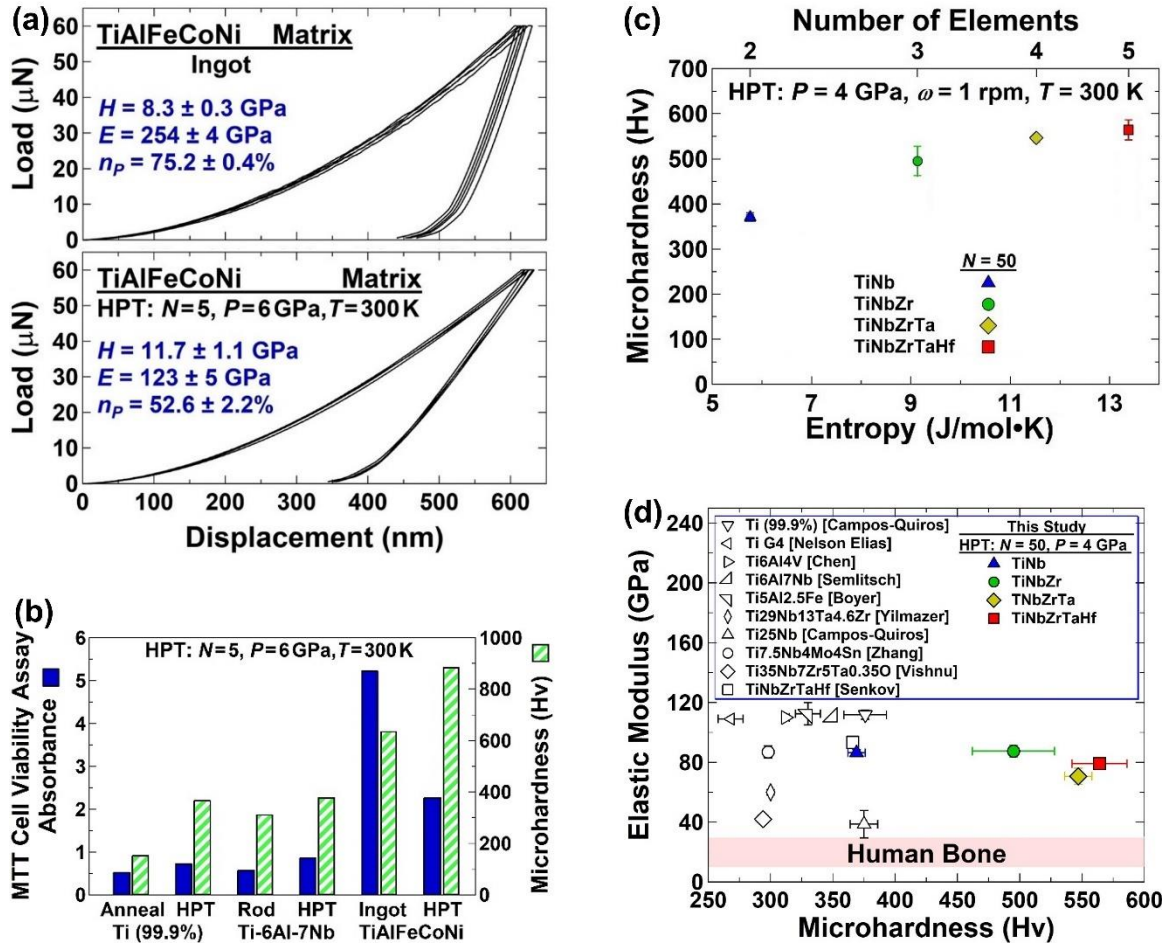


Fig. 3 Development of high-entropy alloys with high strength, high biocompatibility and low elastic modulus by severe plastic deformation. **a** Nanoindentation load against displacement for TiAlFeCoNi after arc melting (ingot) and HPT processing. Reproduced with permission from Ref. [123]. Copyright 2020, Elsevier. **b** Biocompatibility, examined by MTT cell viability assay, and hardness of ingot and HPT-processed TiAlFeCoNi samples in comparison with pure titanium after annealing and HPT processing and Ti-6Al-7Nb (wt.%) after extrusion (rod) and HPT processing. Reproduced with permission from Ref. [123]. Copyright 2020, Elsevier. **c** Hardness against configurational entropy and the number of elements for TiNb, TiNbZr, TiNbZrTa and TiNbZrTaHf synthesized by HPT. Reproduced with permission from Ref. [134]. Copyright 2021, Elsevier. **d** Elastic modulus and hardness of TiNb, TiNbZr, TiNbZrTa and TiNbZrTaHf synthesized by HPT in comparison with some conventional biomaterials and human bone. Reproduced with permission from Ref. [134]. Copyright 2021, Elsevier.

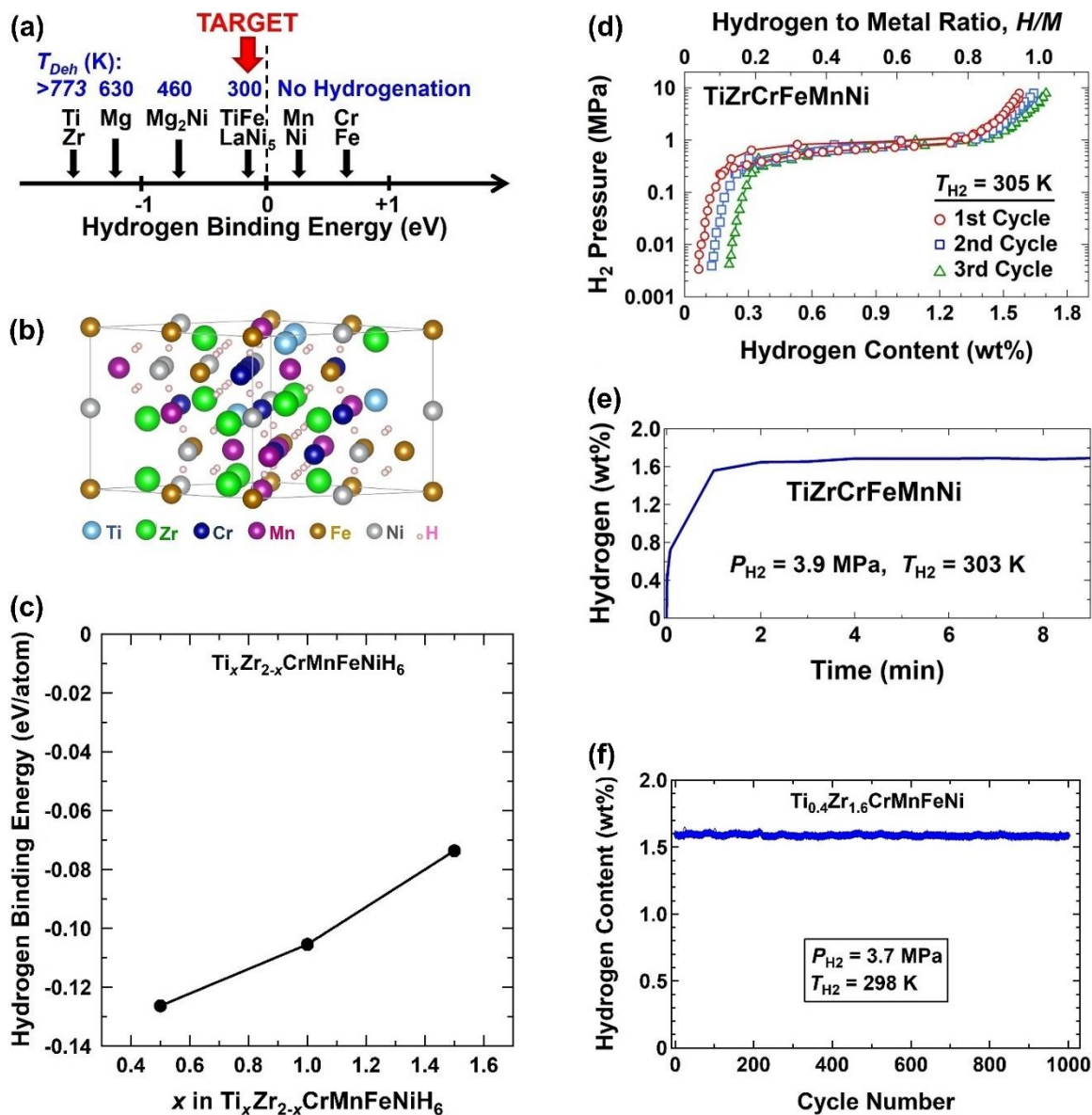


Fig. 4 Design of high-entropy alloys with fast and reversible hydrogen storage at room temperature by binding-energy engineering. **a** Illustration of the concept of hydrogen-binding energy to design room-temperature hydrogen storage materials. Reproduced with permission from Ref. [233]. Copyright 2020, Elsevier. **b** Superlattice of high-entropy hydride $Ti_{0.4}Zr_{1.6}CrMnFeNiH_6$. Reproduced with permission from Ref. [236]. Copyright 2022, Elsevier. **c** Hydrogen binding energy versus titanium content in $Ti_xZr_{2-x}CrMnFeNiH_6$ calculated by first-principles calculations. Reproduced with permission from Ref. [236]. Copyright 2022, Elsevier. **d** Hydrogen pressure-temperature-composition isotherms at room temperature for $TiZrCrMnFeNi$. Reproduced with permission from Ref. [113]. Copyright 2020, Elsevier. **e** Hydrogen content versus hydrogenation time for $TiZrCrMnFeNi$ at room temperature. Reproduced with permission from Ref. [113]. Copyright 2020, Elsevier. **f** Hydrogen storage content during cycling test for $Ti_{0.4}Zr_{1.6}CrMnFeNi$ at room temperature. Reproduced with permission from Ref. [236]. Copyright 2022, Elsevier.

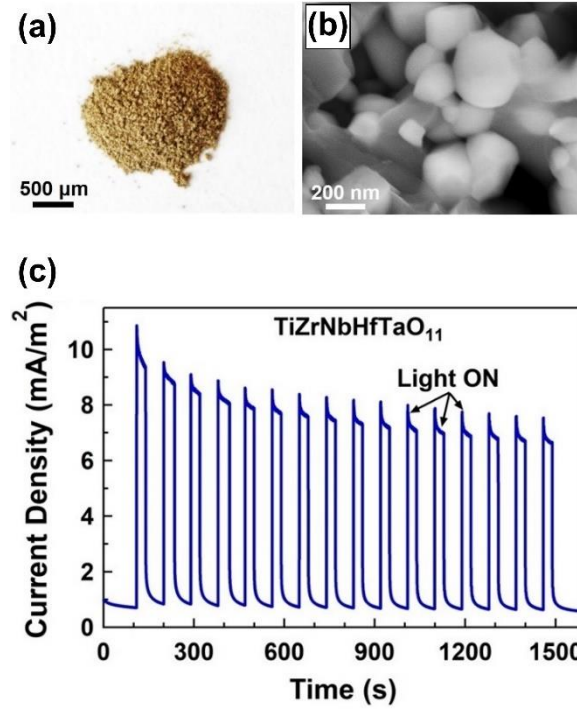


Fig. 5 High-entropy ceramic semiconductors as photovoltaic materials. **a, b** Appearance **b** microstructure visualized by scanning electron microscopy of TiZrZrNbTaO₁₁ synthesized by HPT followed by oxidation. Reproduced with permission from Ref. [126]. Copyright 2020, RCS. **c** Photocurrent generation on TiZrZrNbTaO₁₁. Reproduced with permission from Ref. [155]. Copyright 2022, Elsevier.

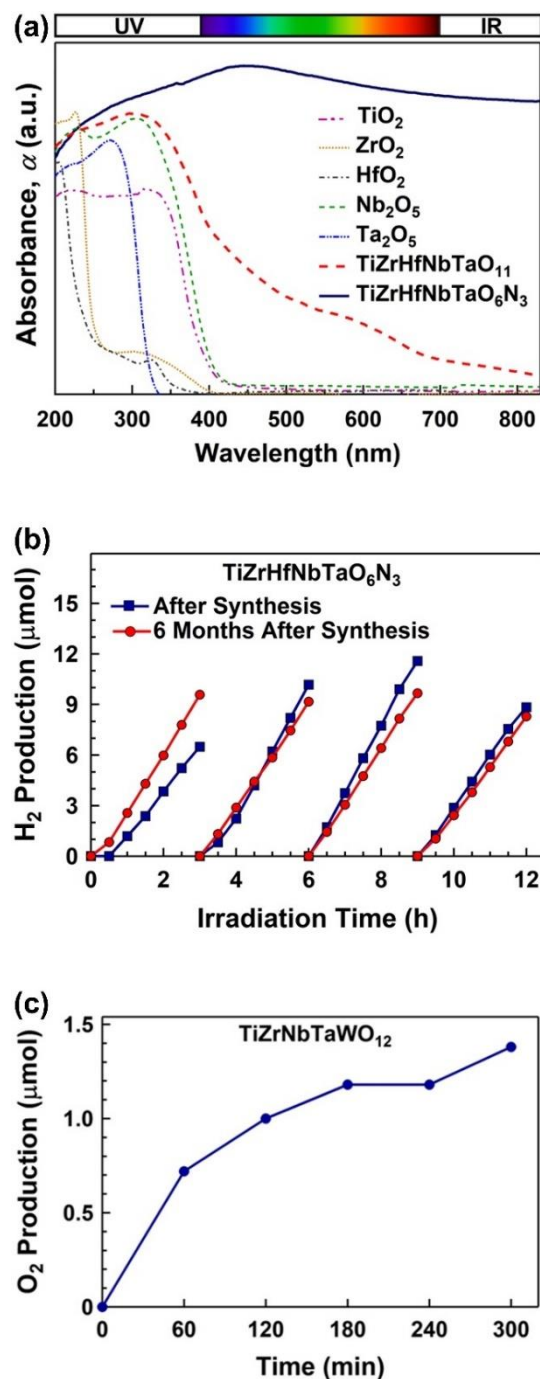


Fig. 6 Photocatalytic water splitting on high-entropy oxides and oxynitrides synthesized by severe plastic deformation. **a** UV-vis light absorbance spectra for TiZrHfNbTaO_{11} and $\text{TiZrHfNbTaO}_6\text{N}_3$ in comparison with binary oxides. Reproduced with permission from Ref. [127]. Copyright 2021, RCS. **b** Photocatalytic hydrogen production under UV light on $\text{TiZrHfNbTaO}_6\text{N}_3$ for four cycles after synthesis and after six-month storage. Reproduced with permission from Ref. [127]. Copyright 2021, RCS. **c** Photocatalytic oxygen production on TiZrNbTaWO_{12} with multiple heterojunctions under visible light. Reproduced with permission from Ref. [160]. Copyright 2022, Elsevier.

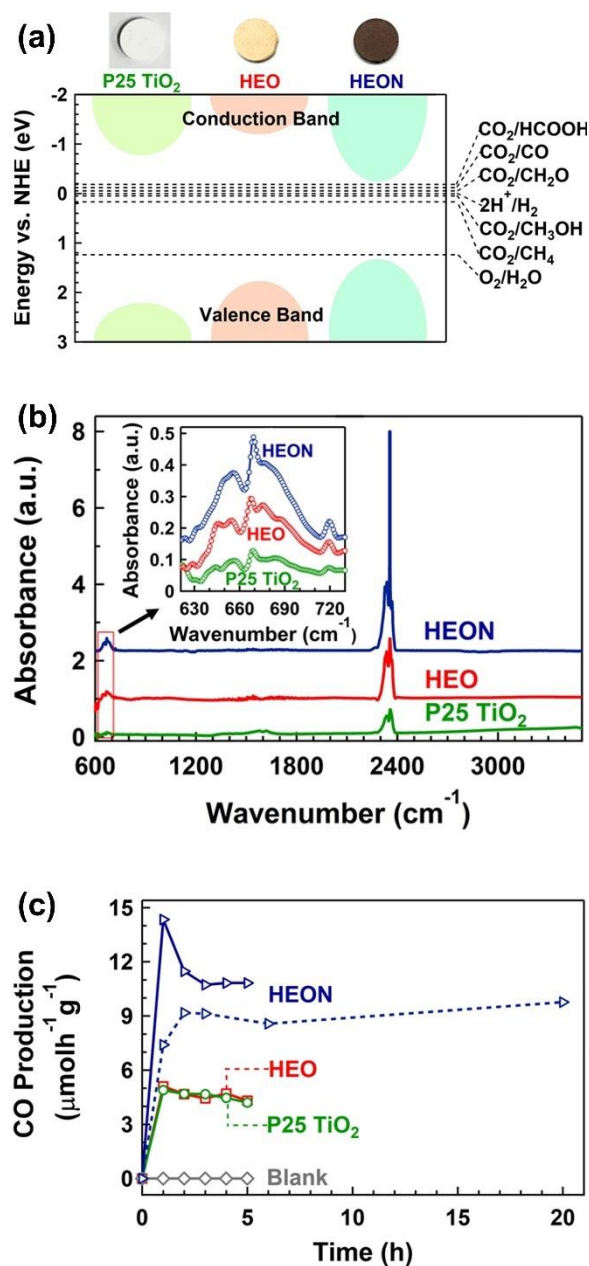


Fig. 7 CO₂ photoreduction to CO on high-entropy oxides and oxynitrides synthesized by severe plastic deformation. **a** Electronic band structure and the appearance of TiZrHfNbTaO₁₁ and TiZrHfNbTaO₆N₃ in comparison with P25 TiO₂. Reproduced with permission from Ref. [154]. Copyright 2022, Elsevier. **b** Diffuse reflectance infrared Fourier transform spectra for TiZrHfNbTaO₁₁ and TiZrHfNbTaO₃N₆ in comparison with P25 TiO₂ in which peaks at 665 cm⁻¹ and 2350 cm⁻¹ correspond to CO₂ chemisorption and physisorption on the surface of catalyst. Reproduced with permission from Ref. [154]. Copyright 2022, Elsevier. **c** CO₂ photoreduction to CO during UV light illumination time on TiZrHfNbTaO₁₁ and TiZrHfNbTaO₃N₆ in comparison with P25 TiO₂. Reproduced with permission from Ref. [154]. Copyright 2022, Elsevier.